Available online at www.sciencedirect.com
ScienceDirect
Comput. Methods Appl. Mech. Engrg. 349 (2019) 17–44
Computer methods in applied mechanics and engineering
www.elsevier.com/locate/cma

A WENO finite-difference scheme for a new class of Hamilton–Jacobi equations in nonlinear solid mechanics

Victor Lefèvre[a,b], Alvaro Garnica[a], Oscar Lopez-Pamies[a,*]

[a] Department of Civil and Environmental Engineering, University of Illinois, Urbana–Champaign, IL 61801, USA
[b] School of Engineering, Brown University, Providence, RI 02912, USA

Received 6 November 2018; received in revised form 4 February 2019; accepted 10 February 2019
Available online 19 February 2019

Highlights

- A high-order WENO finite-difference scheme is presented for a new HJ equation.
- Accuracy and convergence are assessed by direct comparison with an exact solution.
- The scheme is deployed to probe elastomers filled with ferrofluid inclusions.

Abstract

This paper puts forth a high-order weighted essentially non-oscillatory (WENO) finite-difference scheme to numerically generate the viscosity solution of a new class of Hamilton–Jacobi (HJ) equations that has recently emerged in nonlinear solid mechanics. The solution W of the prototypical version of the HJ equations considered here corresponds physically to the homogenized free energy that describes the macroscopic magneto-electro-elastic response of a general class of two-phase particulate composite materials under arbitrary quasi-static finite deformations, electric fields, and magnetic fields in $N = 2, 3$ dimensions. An important mathematical implication of its physical meaning is that W – although it may exhibit steep gradients – is expected to be at least twice continuously differentiable. This is in contrast to the viscosity solutions of the majority of HJ equations that have appeared in other scientific disciplines, which are merely Lipschitz continuous. Three other defining mathematical features that differentiate this new class of HJ equations from most of the existing HJ equations in the literature are that: (i) their "space" variables are defined over non-periodic unbounded or semi-unbounded domains, (ii) their Hamiltonians depend explicitly on all variables, namely, on the "space" and "time" variables, the "space" derivatives of W, and on the function W itself, and (iii) in general, their integration in "time" needs to be carried out over very long "times". The proposed WENO scheme addresses all these features by incorporating a high-order accurate treatment of the boundaries of the domains of computation and by employing a high-order accurate explicit Runge–Kutta "time" integration that remains stable over very large "time" integration ranges. The accuracy and convergence properties of the proposed scheme are demonstrated by direct comparison with a simple explicit solution W available for the case when the general HJ equation is specialized to model the

* Corresponding author.
E-mail addresses: victor.lefevre@northwestern.edu (V. Lefèvre), garnica2@illinois.edu (A. Garnica), pamies@illinois.edu (O. Lopez-Pamies).

https://doi.org/10.1016/j.cma.2019.02.008

elastic response of isotropic porous Gaussian elastomers. Finally, for showcasing purposes, the scheme is deployed to probe the magneto-elastic response of a novel class of magnetorheological elastomers filled with ferrofluid inclusions.

Keywords: High-order WENO schemes; Flux numerical methods; Exact Hamilton–Jacobi solutions; Porous elastomers; Electromagnetic solids

1. Introduction

This paper introduces a numerical scheme to efficiently generate accurate approximations for the viscosity solution of a novel class of Hamilton–Jacobi (HJ) equations that has recently emerged in nonlinear solid mechanics [1]. Physically, the solution W of the specific type of HJ partial differential equations (PDEs) considered here – which, as elaborated below, is a prototypical version of the general mathematical form of this newly emerged class of equations – corresponds to the homogenized free energy that characterizes the macroscopic *nonlinear* and *coupled* magneto-electro-elastic response of a broad class of two-phase particulate composites under arbitrary finite deformations, electric fields, and magnetic fields in $N = 2, 3$ dimensions. Furthermore, the "space" variables[1] in this type of equations correspond physically to the combined $N^2 + 2N$ components of the deformation gradient tensor $\mathbf{F}$, Lagrangian electric field $\mathbf{E}$, and Lagrangian magnetic field $\mathbf{H}$ describing the applied macroscopic loading, whereas the "time" variable corresponds to the volume fraction c of the underlying inclusions in the composite.

From a mathematical point of view, because of its physical meaning, the solution W is expected to be at least twice continuously differentiable, provided that the free-energy functions characterizing the magneto-electro-elastic behaviors of the matrix material and inclusions making up the composite are sufficiently smooth.[2] This high degree of regularity is of note, as the viscosity solutions of the majority of HJ equations that have appeared in other disciplines are merely Lipschitz continuous; see [2] as well as, e.g., [3,4], and [5]. In addition, the Hamiltonian $\mathcal{H}$ in the new HJ equations of interest here depends *explicitly* not only on all the "space" variables $\mathbf{F}$, $\mathbf{E}$, $\mathbf{H}$, and the associated "space" derivatives $\partial W/\partial \mathbf{F}$, $\partial W/\partial \mathbf{E}$, $\partial W/\partial \mathbf{H}$, but *also* on the "time" variable c and the solution W itself. Because of this general functional dependence of the Hamiltonian – which, much like the high regularity of W, is uncharacteristic of most of the existing HJ equations in the literature – the use of otherwise powerful solution representations to construct numerical approximations for W seems futile; see, e.g., Chapter II in [6], Chapter 10 in [7], and references therein. In this work, in the footsteps of Crandall and Lions [8] and of Osher and Sethian [9], we shall pursue a finite-difference scheme combined with a suitably selected numerical Hamiltonian in order to construct numerical approximations for W at the vertices of a Cartesian grid in "space" and "time". Aimed at putting forth a robust and efficient scheme capable of high accuracy, we make use in particular of a WENO (weighted essentially non-oscillatory) finite-difference scheme of high order to discretize the relevant derivatives in "space", together with a high-order explicit Runge–Kutta scheme for the "time" integration.

To put the present contribution into context, we should mention that there are several works in the literature – starting with Jiang and Peng [10] and Bryson and Levy [11] – that have proposed schemes for multi-dimensional HJ equations in the same spirit as the one that we propose here. In contrast to the schemes introduced in those works, because of the physical nature of the HJ equations of interest here, our scheme deals with computational domains that are *not* periodic in "space", thereby requiring a suitable extension of the WENO discretization that affords a high-order accurate representation of the "space" derivatives of the solution W in the regions close to the boundaries of the given computational domain. Furthermore, since solutions are desirable for composite materials with all volume fractions of inclusions in the physical range $0 \leq c \leq 1$ – or equivalently, as elaborated further below, for *all* positive "times" $0 \leq t = -\ln c \leq +\infty$ – our scheme must make use of a "time" integration that remains stable and accurate over very long "times". One more point of further contrast, already alluded to above, is the suitability of our scheme to deal with Hamiltonians of general functional dependence. Indeed, the schemes

[1] Throughout this paper, we make use of the standard terminology of "space" and "time" employed in the literature to refer to the independent variables in HJ equations.

[2] We emphasize that this expectation is mostly *physically* based since, by and large, establishing the regularity of homogenized functionals still remains an open problem. Nevertheless, the few analytical solutions available for W (see, e.g., Section 4) happen to indeed be at least twice continuously differentiable.

currently available in the literature have been tested primarily for multi-dimensional HJ equations wherein the Hamiltonians are independent of the "time" variable and of the unknown function itself; see, e.g., [10–12].

The remainder of the paper is organized as follows. We begin in Section 2 by introducing the class of HJ equations of interest in this work. In Section 3, we present the scheme to construct numerical approximations for the viscosity solution W of such a class of PDEs. We devote Section 4 to discussing the accuracy and convergence properties of the proposed numerical scheme. This is done within the physical context of the elastic response of isotropic porous Gaussian (or Neo-Hookean) elastomers, for which the relevant HJ equation admits a simple explicit solution. Finally, for showcasing purposes, we put to use in Section 5 the proposed scheme in order to generate results for the macroscopic response of a new class of magnetorheological elastomers, those comprising an elastomer filled with ferrofluid inclusions.

2. A new class of HJ equations in nonlinear solid mechanics

In contrast to their repeated and pervasive appearance in many other scientific disciplines, such as, for instance, geometrical optics, semi-classical quantum mechanics, control theory, and level-set methods [see, e.g., 4,13–15], HJ equations have only emerged recently in the field of solid mechanics. They have done so from the combination of iterated dilute homogenization techniques [16–18] with the celebrated homogenization results for coated laminates [19,20] in the derivation of the macroscopic nonlinear constitutive properties of composite materials with certain classes of two-phase particulate microstructures. In point of fact, following the seminal work of deBotton [21], a HJ equation was first derived by Idiart [22] in the context of small-strain nonlinear elasticity. This HJ equation was later generalized to finite elasticity by Lopez-Pamies and Idiart [23,24] and Lopez-Pamies et al. [25]. A further generalization with deeper conceptual implications was introduced subsequently in [1]. Indeed, beyond revealing its applicability to the coupling between balance of momenta and Maxwell's equations, the derivation presented by Lopez-Pamies [1] in the context of electroelastostatics served to reveal more generally that the same type of HJ equation would emerge in the derivation of the macroscopic nonlinear and coupled constitutive response of composite materials – again, with certain classes of two-phase particulate microstructures – under any number of different (not just mechanical and electric) fields, so long as these fields satisfy conservation laws. In this paper, for definiteness, we shall concern ourselves with such a general type of HJ equation written in the context of magneto-electro-elastostatics. Precisely, we shall consider the following HJ equation for the function $W = W(\mathbf{F}, \mathbf{E}, \mathbf{H}, c)$:

$$\begin{cases} \dfrac{\partial W}{\partial \mathtt{c}} + \mathcal{H}\left(\mathbf{F}, \mathbf{E}, \mathbf{H}, \mathtt{c}, W, \dfrac{\partial W}{\partial \mathbf{F}}, \dfrac{\partial W}{\partial \mathbf{E}}, \dfrac{\partial W}{\partial \mathbf{H}}\right) = 0, \quad \{\mathbf{F}, \mathbf{E}, \mathbf{H}\} \in \mathfrak{S}, \quad \mathtt{c} \in \mathfrak{T} \\ W(\mathbf{F}, \mathbf{E}, \mathbf{H}, 1) = W_{\mathtt{i}}(\mathbf{F}, \mathbf{E}, \mathbf{H}), \quad \{\mathbf{F}, \mathbf{E}, \mathbf{H}\} \in \mathfrak{S} \end{cases}, \tag{1}$$

where $\mathfrak{S} = \{\mathbf{A} \in \mathbb{R}^{N\times N} : \det \mathbf{A} > 0\} \times \mathbb{R}^N \times \mathbb{R}^N$ and $\mathfrak{T} = [c, 1)$, with Hamiltonian

$$\mathcal{H} = -\frac{1}{\mathtt{c}} W - \frac{1}{\mathtt{c}} \int_{|\boldsymbol{\xi}|=1} \max_{\boldsymbol{\alpha}} \min_{\beta,\gamma} \left[\alpha_i \frac{\partial W}{\partial F_{ij}} \xi_j + \beta \frac{\partial W}{\partial E_i} \xi_i + \gamma \frac{\partial W}{\partial H_i} \xi_i \right.$$
$$\left. - W_{\mathtt{m}}(\mathbf{F} + \boldsymbol{\alpha} \otimes \boldsymbol{\xi}, \mathbf{E} + \beta\boldsymbol{\xi}, \mathbf{H} + \gamma\boldsymbol{\xi}) \right] \nu(\boldsymbol{\xi}) \mathrm{d}\boldsymbol{\xi}, \tag{2}$$

$i, j = 1, \ldots, N$. In these expressions, as mentioned in the Introduction, $\mathbf{F}$, $\mathbf{E}$, and $\mathbf{H}$ denote the macroscopic deformation gradient, macroscopic Lagrangian electric field, and macroscopic Lagrangian magnetic field applied to a two-phase particulate composite material occupying the open domain $\Omega_0 \subset \mathbb{R}^N$ $(N = 2, 3)$ in its undeformed, unpolarized, and unmagnetized configuration, wherein the magneto-electro-elastic response of the matrix and inclusions are characterized by the "total" free-energy functions $W_{\mathtt{m}}$ and $W_{\mathtt{i}}$, respectively, and whose microstructure is characterized by the volume fraction of inclusions c in Ω_0 and the variable $\nu = \nu(\boldsymbol{\xi})$. For the case of random[3] distributions of inclusions, in terms of the one- and two-point correlation functions $p_0^{(\mathtt{i})}$ and $p_0^{(\mathtt{ii})} = p_0^{(\mathtt{ii})}(\mathbf{X})$, $\mathbf{X} \in \Omega_0$, describing the spatial distribution of the inclusions in Ω_0, we have the explicit connections

$$c = p_0^{(\mathtt{i})} \qquad \text{and} \qquad \nu(\boldsymbol{\xi}) = \frac{1}{(2\pi)^N} \int_{\Omega_0} \int_0^\infty \frac{p_0^{(\mathtt{ii})}(\mathbf{X}) - c^2}{c(1-c)} \rho^{N-1} e^{i\rho\boldsymbol{\xi}\cdot\mathbf{X}} \, \mathrm{d}\rho \, \mathrm{d}\mathbf{X}, \tag{3}$$

[3] In this paper, attention is restricted to composite materials wherein the distribution of inclusions is random. For the case of periodic microstructures, we still have $c = p_0^{(\mathtt{i})}$, but the function $\nu(\boldsymbol{\xi})$ is given in terms of c and $p_0^{(\mathtt{ii})}$ by expressions other than $(3)_2$; see Appendix A in [1].

where $i = \sqrt{-1}$.

The following remarks are in order:

i. *Physical meaning of the HJ equation* (1)–(2). As already announced in the Introduction, the viscosity solution W of the HJ equation (1)–(2) corresponds to the homogenized "total" free energy characterizing the macroscopic magneto-electro-elastic response of a general class of two-phase particulate composites. The coupled constitutive relation implied by W is simply given by its partial derivatives with respect to its three first arguments [26,27], namely,

$$\mathbf{S} = \frac{\partial W}{\partial \mathbf{F}}(\mathbf{F}, \mathbf{E}, \mathbf{H}, c), \qquad \mathbf{D} = -\frac{\partial W}{\partial \mathbf{E}}(\mathbf{F}, \mathbf{E}, \mathbf{H}, c), \qquad \text{and} \qquad \mathbf{B} = -\frac{\partial W}{\partial \mathbf{H}}(\mathbf{F}, \mathbf{E}, \mathbf{H}, c), \tag{4}$$

where $\mathbf{S}$, $\mathbf{D}$, and $\mathbf{B}$ stand, respectively, for the macroscopic first Piola–Kirchhoff stress, macroscopic Lagrangian electric displacement field, and macroscopic Lagrangian magnetic induction.

We emphasize that the result (1)–(2) is valid for any (suitably well behaved) free-energy functions $W_{\mathtt{m}}$ and $W_{\mathtt{i}}$ of choice describing the magneto-electro-elastic behaviors of the underlying matrix and inclusions. These include an admittedly broad spectrum of materials, ranging from materials with odd electroelastic and/or magnetoelastic coupling such as piezoelectric, piezomagnetic, or magnetoelectric materials to those with even electroelastic and/or magnetoelastic coupling such as electrostrictive and magnetostrictive materials.

The result (1)–(2) is also valid for any choice of volume fraction of inclusions in the range $c \in [0, 1]$ and any choice of the two-point correlation function $p_0^{(\mathtt{ii})}$ describing their distribution. The fact that $c \in [0, 1]$ brings into view that the result (1)–(2) corresponds to composite materials with particulate microstructures wherein the inclusions are polydisperse in size. Their possibly anisotropic shape and spatial arrangement are dictated by the choice of $p_0^{(\mathtt{ii})}$.

ii. *The use of* (1)–(2) *as an analytical tool to investigate fundamental problems*. In addition to its theoretical value in providing a rigorous – albeit implicit – homogenization solution for the *nonlinear* and *coupled* response of composite materials with a fairly general class of particulate microstructures, the HJ equation (1) with (2) provides, by the same token, a formidable practical tool to investigate a wide range of fundamental phenomena.

For example, in the absence of electric and magnetic fields (i.e., when $\mathbf{E} = \mathbf{0}$ and $\mathbf{H} = \mathbf{0}$), the PDE (1) with (2) has enabled the construction of a closed-form solution for the homogenization problem of the elastic response of Gaussian rubber containing a dilute distribution of vacuous cavities, or point defects, which in turn has led to the formulation of a new framework to determine the onset of cavitation instabilities in rubber subjected to arbitrary loading conditions [28,29]. It has also enabled the construction of a closed-form solution for the parallel fundamental homogenization problem of the elastic response of Gaussian rubber filled by a dilute isotropic distribution of rigid particles under arbitrarily large deformations [30].

In the presence of an electric field but in the absence of a magnetic field (i.e., when $\mathbf{E} \neq \mathbf{0}$ and $\mathbf{H} = \mathbf{0}$), the PDE (1)–(2) has also been utilized recently to generate closed-form solutions for the macroscopic electromechanical response of both piezoelectric composites and ideal elastic dielectric composites in the "classical" limit of small deformations and moderate electric fields [31,32], as well as in the opposite limit of infinitely large deformations [33]. Because of the well-known mathematical analogy between electroelastostatics and magnetoelastostatics (see, e.g., [34]), the analogous fundamental solutions in the presence of a magnetic field but in the absence of an electric field (i.e., when $\mathbf{H} \neq \mathbf{0}$ and $\mathbf{E} = \mathbf{0}$) have also been recently worked out [35].

The above-cited examples have allowed for *analytical* solutions W of (1)–(2) because they correspond to limiting cases (either $c \to 0+$, $\mathbf{F} \to \mathbf{I}$ and $\mathbf{E} \to \mathbf{0}$, $\mathbf{F} \to \mathbf{I}$ and $\mathbf{H} \to \mathbf{0}$, or $\|\mathbf{F}\| \to +\infty$) amenable to tractable asymptotic analyses. In general, however, the PDE (1)–(2) does *not* admit analytical solutions and requires instead a numerical treatment.

iii. *The use of* (1)–(2) *as a numerical tool to investigate a wider range of fundamental problems*. In order to exploit the full potential of the HJ equation (1)–(2) to investigate fundamental and novel problems in the realm of nonlinear and coupled phenomena, we must be able to generate *numerical* solutions for it. The main objective of this paper is precisely to introduce a numerical scheme to efficiently generate such solutions. Towards this end, it first proves helpful to recognize three of the unique mathematical features of (1)–(2) when compared to existing HJ equations in the literature:

- Because of its physical meaning, the solution W of (1)–(2) is expected to be twice continuously differentiable. Yet, it may exhibit steep gradients, which may prove challenging to resolve numerically;
- While the "space" domain of definition $\mathfrak{S}$ of the HJ equation (1)–(2) is *unbounded* or *semi-unbounded*, numerical solutions can of course only be generated on a given computational domain $\mathfrak{S}^h \subset \mathfrak{S}$ of *finite* extent, with *finite* boundary $\partial\mathfrak{S}^h$. This poses two significant challenges. The first one is that extra boundary conditions may need to be provided on the whole or on parts of any given $\partial\mathfrak{S}^h$ to ensure well-posedness of the discretized equations to be solved. Given that the HJ equation (1)–(2) is *not* periodic in "space", these extra boundary conditions required on $\partial\mathfrak{S}^h$ ought to be generated from the PDE $(1)_1$ itself. The second challenge is that the design of discretization schemes close to $\partial\mathfrak{S}^h$ requires invariably especial treatment, more so if one seeks a stable and high-order accurate scheme;
- The initial condition in (1) is given at $\mathtt{c} = c = 1$, which corresponds to the limiting case when the composite material is actually homogeneous and comprised entirely of the inclusion material. Yet, it is desirable to have solutions W for composite materials with the entire range of volume fractions of inclusions c, including dilute volume fractions when $\mathtt{c} = c = 0+$. As elaborated further below, this effectively requires integrating the PDE (1)–(2) over very long "times", which in turn requires the use of robust "time" integration schemes that remain stable and accurate over very large "time" integration ranges.

iv. *The use of (1)–(2) as a testbed to critically assess HJ-equation solvers.* Before proceeding with the presentation of the numerical scheme *per se*, it is worth remarking that because of the mathematical features outlined in the preceding remark, together with the general functional dependence of the Hamiltonian (2), the HJ equation (1)–(2) provides a natural testbed, physically meaningful and mathematically challenging, for the investigation of the performance of numerical schemes aimed at solving HJ equations. In particular, the existence of simple explicit solutions W of the HJ equation (1)–(2) for some specific choices of free-energy functions $W_{\mathtt{m}}$, $W_{\mathtt{i}}$ and loading conditions $\mathbf{F}$, $\mathbf{E}$, $\mathbf{H}$ allows for the straightforward investigation of the accuracy and convergence properties of these schemes. We carry out such an investigation below in Section 4 for the numerical scheme that we propose here.

3. The proposed WENO finite-difference scheme for the HJ equation (1)–(2)

At this stage, we are in a position to proceed with the presentation of the scheme to generate numerical approximations for the viscosity solution W of the HJ equation (1)–(2). In a nutshell, following the footsteps of Crandall and Lions [8], the scheme consists of the discrete "time" integration of a suitably selected numerical Hamiltonian, so as to construct at the vertices of a Cartesian grid (in "space") successive (in "time") numerical approximations of W. With the objective of putting forth a scheme that is robust and capable of delivering high accuracy even when W exhibits steep gradients, combining ideas from the works of Osher and Sethian [9] and of Jiang and Shu [36], we make use in particular of fifth-order accurate WENO finite-difference approximations of the "space" derivatives of W, together with a fifth-order accurate explicit Runge–Kutta "time" integration. We begin in Section 3.1 by introducing some helpful notation, and by outlining the definition and features of the proposed WENO approximation for a multivariable scalar-valued function, both for "interior" and "boundary" grid points of any given finite computational domain. In Section 3.2, we lay out the "space" discretization of the HJ equation (1)–(2) in terms of the WENO approximation introduced in Section 3.1. In turn, in Section 3.3, we spell out the "time" discretization of the "spatially" discretized equations put forth in Section 3.2. We close in Section 3.4 by summarizing the whole of the proposed scheme and by recording a number of practical remarks on its numerical implementation.

3.1. WENO approximation of the first partial derivatives of a scalar-valued function over a finite domain

Borrowing ideas from the pioneering work of Liu et al. [37] on WENO finite-volume schemes, WENO finite-difference schemes were first introduced by Jiang and Shu [36] in the context of hyperbolic conservation laws. Over the last two decades, they have become an increasingly popular method of choice to solve numerically convection dominated problems. The defining feature of the WENO framework is that it enables a discretized representation of the (partial) derivatives of a (multi-variable) function with arbitrarily-high accuracy, at least formally, in the smooth

regions of the function, while it approximates them in a non-oscillatory manner where the function is discontinuous or exhibits steep gradients. For additional details on WENO schemes, including an overview of their increasing application to a broad range of physical problems, we refer the interested reader to the comprehensive review of Shu [38].

3.1.1. WENO approximation of the first derivative of a single-variable function

For clarity of exposition, as a prologue to the "space" discretization of the HJ equation (1)–(2), we begin by presenting fifth-order accurate *left-biased* and *right-biased* WENO approximation formulas for the first derivative $u_x(x) = \mathrm{d}u(x)/\mathrm{d}x$ of a generic single-variable function $u(x)$ in terms of its values $u_i = u(x_i)$ at the $M+1$ evenly-spaced vertices of a 1D Cartesian grid,[4] that is, $\mathfrak{S}^h = \{x_i : x_i = x_0 + ih, 0 \le i \le M\}$. These formulas will then be generalized to the first partial derivatives of a generic multivariable function.

The left-biased WENO approximation. We consider for a given grid point x_i, $3 \le i \le M-2$, the four-point stencil $S_1^- = \{x_{i-3}, x_{i-2}, x_{i-1}, x_i\}$. The derivative $\mathrm{d}p_1^-(x)/\mathrm{d}x$ of the unique Lagrange polynomial $p_1^-(x)$ that interpolates $u(x)$ over the stencil S_1^- is used to approximate the first derivative $u_x(x)$ of $u(x)$ on S_1^-; see, e.g., Chapter 1 in LeVeque [39]. In particular, assuming that the function $u(x)$ is (sufficiently) smooth in S_1^-, we have at the grid point $x = x_i$ that

$$u_x(x_i) = u_{x,i}^{-,1} + O(h^3),$$

where

$$u_{x,i}^{-,1} = \frac{\mathrm{d}p_1^-}{\mathrm{d}x}(x_i) = \frac{1}{3}\frac{\Delta^+ u_{i-3}}{h} - \frac{7}{6}\frac{\Delta^+ u_{i-2}}{h} + \frac{11}{6}\frac{\Delta^+ u_{i-1}}{h}; \tag{5}$$

here and subsequently, we make use of the notation $\Delta^+ v_k = v_{k+1} - v_k$. Similarly, the interpolating polynomial $p_2^-(x)$ on the second stencil $S_2^- = \{x_{i-2}, x_{i-1}, x_i, x_{i+1}\}$ results in the approximation

$$u_x(x_i) = u_{x,i}^{-,2} + O(h^3),$$

where

$$u_{x,i}^{-,2} = \frac{\mathrm{d}p_2^-}{\mathrm{d}x}(x_i) = -\frac{1}{6}\frac{\Delta^+ u_{i-2}}{h} + \frac{5}{6}\frac{\Delta^+ u_{i-1}}{h} + \frac{1}{3}\frac{\Delta^+ u_i}{h}, \tag{6}$$

granted, again, that the function $u(x)$ is smooth in S_2^-. Considering the third stencil $S_3^- = \{x_{i-1}, x_i, x_{i+1}, x_{i+2}\}$ involves yet a different interpolating polynomial $p_3^-(x)$ such that

$$u_x(x_i) = u_{x,i}^{-,3} + O(h^3),$$

where

$$u_{x,i}^{-,3} = \frac{\mathrm{d}p_3^-}{\mathrm{d}x}(x_i) = \frac{1}{3}\frac{\Delta^+ u_{i-1}}{h} + \frac{5}{6}\frac{\Delta^+ u_i}{h} - \frac{1}{6}\frac{\Delta^+ u_{i+1}}{h}, \tag{7}$$

provided again that the function $u(x)$ is smooth in S_3^-.

Having generated the third-order accurate approximations (5)–(7), the left-biased WENO approximation of $u_x(x_i)$ is defined as the following weighted average:

$$u_{x,i}^- = \omega_1 u_{x,i}^{-,1} + \omega_2 u_{x,i}^{-,2} + \omega_3 u_{x,i}^{-,3}, \tag{8}$$

where the weights ω_1, ω_2, ω_3, which satisfy the standard condition $\omega_1 + \omega_2 + \omega_3 = 1$, are to be selected so that:

1. If the function $u(x)$ is smooth in the combined six-point stencil $S^- = \{x_{i-3}, x_{i-2}, x_{i-1}, x_i, x_{i+1}, x_{i+2}\}$, then
$$\omega_1 = \frac{1}{10} + O(h^2), \quad \omega_2 = \frac{3}{5} + O(h^2), \quad \omega_3 = \frac{3}{10} + O(h^2).$$
2. If the function $u(x)$ contains a singularity or a steep gradient in the stencil S_j^-, and is smooth in at least one of the other two stencils, then
$$\omega_j = 0 + O(h^3).$$

[4] Such grids will later serve as computational domains for the computation of solutions of the HJ equation (1)–(2). We therefore denote by $\mathfrak{S}^h$ Cartesian grids and computational domains alike and by $\partial\mathfrak{S}^h$ their boundaries.

The above two requirements entail that in regions where the function $u(x)$ is smooth, the left-biased WENO approximation (8) of $u_x(x_i)$ is fifth-order accurate, more specifically,

$$u^-_{x,i} = \frac{1}{30}\frac{\Delta^+ u_{i-3}}{h} - \frac{13}{60}\frac{\Delta^+ u_{i-2}}{h} + \frac{47}{60}\frac{\Delta^+ u_{i-1}}{h} + \frac{9}{20}\frac{\Delta^+ u_i}{h} - \frac{1}{20}\frac{\Delta^+ u_{i+1}}{h} + O(h^5).$$

On the other hand, in regions where the function $u(x)$ contains a singularity or a steep gradient, the expression (8) renders a nonoscillatory (at least) third-order accurate left-biased WENO approximation of $u_x(x_i)$.

Sets of weights that are consistent with the above two requirements are not unique. In this work, we shall make use of weights within the class of those proposed by Jiang and Shu [36] in the context of conservation laws. They are defined as follows:

$$\omega_j = \frac{\widetilde{\omega}_j}{\widetilde{\omega}_1 + \widetilde{\omega}_2 + \widetilde{\omega}_3} \quad \text{with} \quad \widetilde{\omega}_j = \frac{\gamma_j}{(\epsilon + \mathcal{S}_j)^2} \qquad 1 \le j \le 3, \tag{9}$$

where

$$\gamma_1 = \frac{1}{10}, \quad \gamma_2 = \frac{3}{5}, \quad \gamma_3 = \frac{3}{10}, \tag{10}$$

$$\begin{aligned}\mathcal{S}_j &= \sum_{l=2}^{3} h^{2l-1} \int_{x_i - \frac{1}{2}h}^{x_i + \frac{1}{2}h} \left(\frac{\mathrm{d}^l p_j^-}{\mathrm{d}x^l}\right)^2 \mathrm{d}x \\ &= \frac{13}{12}\left(\Delta^-\Delta^+ u_{i+j-3} - \Delta^-\Delta^+ u_{i+j-2}\right)^2 + \left[(j-2)\Delta^-\Delta^+ u_{i+j-3} - (j-3)\Delta^-\Delta^+ u_{i+j-2}\right]^2,\end{aligned} \tag{11}$$

and where the notation $\Delta^- v_k = v_k - v_{k-1}$ has been utilized for subsequent convenience. In $(9)_2$, ϵ is a small real number which is introduced to avoid vanishingly small denominators; for the PDEs of interest here, numerical tests indicate that $\epsilon = 10^{-12}$ is an adequate choice.[5] The parameters $\mathcal{S}_j$ defined in (11) are scaled sums of the squared L^2-norms of the second and third derivatives of the interpolating polynomials p_j^-, $1 \le j \le 3$ and serve as indicators of the smoothness of $u_x(x)$: the larger the value of $\mathcal{S}_j$, the lesser the smoothness of the function $u_x(x)$ in the stencil S_j^-. The interested reader is referred to Jiang and Shu [36] and Henrick et al. [40] for further details on the above and other weights.

Granted the choice of weights (9)–(11), the left-biased WENO approximation (8) of $u_x(x_i)$, $3 \le i \le M-2$, can be rewritten in the more compact form

$$\begin{aligned}u^-_{x,i} = &-\frac{1}{12}\frac{\Delta^+ u_{i-2}}{h} + \frac{7}{12}\frac{\Delta^+ u_{i-1}}{h} + \frac{7}{12}\frac{\Delta^+ u_i}{h} - \frac{1}{12}\frac{\Delta^+ u_{i+1}}{h} - \\ &g\left(\frac{\Delta^-\Delta^+ u_{i-2}}{h}, \frac{\Delta^-\Delta^+ u_{i-1}}{h}, \frac{\Delta^-\Delta^+ u_i}{h}, \frac{\Delta^-\Delta^+ u_{i+1}}{h}\right),\end{aligned} \tag{12}$$

where

$$g(z_1, z_2, z_3, z_4) = \frac{1}{3}\widehat{\omega}_1 (z_1 - 2z_2 + z_3) + \frac{1}{6}(\widehat{\omega}_3 - \frac{1}{2})(z_2 - 2z_3 + z_4) \tag{13}$$

with

$$\widehat{\omega}_j = \frac{\dfrac{\gamma_j}{(\epsilon + h^2\widehat{\mathcal{S}}_j)^2}}{\sum_{k=1}^{3} \dfrac{\gamma_k}{(\epsilon + h^2\widehat{\mathcal{S}}_k)^2}}, \quad \widehat{\mathcal{S}}_j = \frac{13}{12}(z_j - z_{j+1})^2 + \left[(j-2)z_j - (j-3)z_{j+1}\right]^2, \quad 1 \le j \le 3, \tag{14}$$

where the explicit dependence of $\widehat{\omega}_j$ and $\widehat{\mathcal{S}}_j$ on $z_1, \ldots, z_4$ has been omitted for notational convenience and where we recall that the constant parameters γ_1, γ_2, γ_3 are given by (10).

Boundary treatment. The WENO approximation (12) of $u_x(x_i)$ requires knowledge of the value of $u(x)$ at a number of grid points adjacent to x_i, precisely, the point values u_j, $i-3 \le j \le i+2$. As a result, the WENO expression (12) is only valid for "interior" grid points sufficiently away from the boundary $\partial\mathfrak{S}^h$, precisely, the grid points x_i, $3 \le i \le M-2$. Howbeit, the same construction process presented above can be utilized to construct a corresponding

[5] Based on the study of Henrick et al. [40], this value is selected so as to not interfere with the overall convergence rate of the scheme.

fifth-order accurate left-biased WENO approximation for the "boundary" grid points, that is, the five remaining grid points x_0, x_1, x_2, x_{M-1}, x_M located too close to $\partial\mathfrak{S}^h$ for (12) to be used. We present next the derivation of such a WENO approximation for the outermost left grid point x_0. The corresponding results for the other four "boundary" grid points x_1, x_2, x_{M-1}, x_M are placed on record in Appendix A.

For the "boundary" grid point x_0, we hence consider the unique Lagrange polynomials $p_k^-(x)$, $4 \leq k \leq 6$, interpolating $u(x)$ on each of the three four-point stencils $S_k^- = \{x_{k-4}, x_{k-3}, x_{k-2}, x_{k-1}\}$, so that provided that $u(x)$ is (sufficiently) smooth in S_k^-,

$$u_x(x_0) = u_{x,0}^{-,k} + O(h^3)$$

with

$$\begin{aligned}
u_{x,0}^{-,4} &= \frac{\mathrm{d}p_4^-}{\mathrm{d}x}(x_0) = \frac{11}{6}\frac{\Delta^+ u_0}{h} - \frac{7}{6}\frac{\Delta^+ u_1}{h} + \frac{1}{3}\frac{\Delta^+ u_2}{h},\\
u_{x,0}^{-,5} &= \frac{\mathrm{d}p_5^-}{\mathrm{d}x}(x_0) = \frac{13}{3}\frac{\Delta^+ u_1}{h} - \frac{31}{6}\frac{\Delta^+ u_2}{h} + \frac{11}{6}\frac{\Delta^+ u_3}{h},\\
u_{x,0}^{-,6} &= \frac{\mathrm{d}p_6^-}{\mathrm{d}x}(x_0) = \frac{47}{6}\frac{\Delta^+ u_2}{h} - \frac{67}{6}\frac{\Delta^+ u_3}{h} + \frac{13}{3}\frac{\Delta^+ u_4}{h}.
\end{aligned} \tag{15}$$

In contrast to the preceding derivation for the "interior" grid points, we remark here that the interpolating polynomials $p_k^-(x)$, $5 \leq k \leq 6$ are used to extrapolate the value of the function $u(x)$ at the grid point of interest x_0 from its values at grid points x_i, $1 \leq i \leq 5$.

Much like for the "interior" grid points, given the third-order approximations (15), the left-biased WENO approximation of $u_x(x_0)$ is then defined as the weighted average

$$u_{x,0}^- = \omega_{4,0} u_{x,0}^{-,4} + \omega_{5,0} u_{x,0}^{-,5} + \omega_{6,0} u_{x,0}^{-,6}. \tag{16}$$

Here, the weights $\omega_{4,0}$, $\omega_{5,0}$, $\omega_{6,0}$ add up to 1 and must be selected so that (16) is accurate up to fifth order if $u(x)$ is smooth in the combined six-point stencil $\{x_0, \ldots, x_5\}$, but still provides a non-oscillatory (at least) third-order accurate approximation if $u(x)$ contains a discontinuity or exhibits a steep gradient. Consistent with these requirements, we propose the following set of weights:

$$\omega_{j,0} = \frac{\widetilde{\omega}_{j,0}}{\widetilde{\omega}_{4,0} + \widetilde{\omega}_{5,0} + \widetilde{\omega}_{6,0}} \quad \text{with} \quad \widetilde{\omega}_{j,0} = \frac{\gamma_{j,0}}{(\epsilon + \mathcal{S}_{j,0})^2} \qquad 4 \leq j \leq 6, \tag{17}$$

where

$$\gamma_{4,0} = \frac{137}{110}, \quad \gamma_{5,0} = -\frac{417}{1430}, \quad \gamma_{6,0} = \frac{3}{65}, \tag{18}$$

and where the corresponding smoothness indicators are given by

$$\begin{aligned}
\mathcal{S}_{j,0} &= \sum_{l=2}^{3} h^{2l-1} \int_{x_0 - \frac{1}{2}h}^{x_0 + \frac{1}{2}h} \left(\frac{\mathrm{d}^l p_j^-}{\mathrm{d}x^l}\right)^2 \mathrm{d}x\\
&= \frac{13}{12}\left(\Delta^-\Delta^+ u_{j-3} - \Delta^-\Delta^+ u_{j-2}\right)^2 + \left[(j-2)\Delta^-\Delta^+ u_{j-3} - (j-3)\Delta^-\Delta^+ u_{j-2}\right]^2.
\end{aligned} \tag{19}$$

It follows from the choice of weights (17)–(19) that the left-biased WENO approximation (16) of $u_x(x_0)$ can be rewritten more compactly in the form

$$u_{x,0}^- = \frac{13}{3}\frac{\Delta^+ u_1}{h} - \frac{31}{6}\frac{\Delta^+ u_2}{h} + \frac{11}{6}\frac{\Delta^+ u_3}{h} - g_0\left(\frac{\Delta^-\Delta^+ u_1}{h}, \frac{\Delta^-\Delta^+ u_2}{h}, \frac{\Delta^-\Delta^+ u_3}{h}, \frac{\Delta^-\Delta^+ u_4}{h}\right).$$

Here

$$g_0(z_1, z_2, z_3, z_4) = \frac{11}{6}\widehat{\omega}_{4,0}\left(z_1 - 2z_2 + z_3\right) - \frac{13}{3}\widehat{\omega}_{6,0}\left(z_2 - 2z_3 + z_4\right), \tag{20}$$

where

$$\widehat{\omega}_{j,0} = \frac{\dfrac{\gamma_{j,0}}{(\epsilon + h^2\widehat{\mathcal{S}}_{j,0})^2}}{\displaystyle\sum_{k=4}^{6} \frac{\gamma_{k,0}}{(\epsilon + h^2\widehat{\mathcal{S}}_{k,0})^2}}, \quad \widehat{\mathcal{S}}_{j,0} = \frac{13}{12}\left(z_{j-3} - z_{j-2}\right)^2 + \left[(j-2)z_{j-3} - (j-3)z_{j-2}\right]^2, \tag{21}$$

and where the explicit dependence of $\widehat{\omega}_{j,0}$ and $\widehat{\mathcal{S}}_{j,0}$ on $z_1, \ldots, z_4$ has been omitted for notational convenience and the weights $\gamma_{j,0}$, $4 \leq j \leq 6$ are given by (18).

The derivations of the left-biased WENO approximations of $u_x(x_1)$, $u_x(x_2)$, $u_x(x_{M-1})$, $u_x(x_M)$ follow analogous steps to those presented above and are therefore not repeated here. Instead, once more, the expressions for these approximations are directly reported in Appendix A.

The right-biased WENO approximation. Making use of symmetry arguments, given the four-point stencils $S_k^+ = \{x_{i-k+1}, x_{i-k+2}, x_{i-k+3}, x_{i-k+4}\}$, $1 \leq k \leq 3$, and the combined six-point stencil $S^+ = \{x_{i-2}, x_{i-1}, x_i, x_{i+1}, x_{i+2}, x_{i+3}\}$, the right-biased WENO approximation $u_{x,i}^+$ of $u_x(x_i)$ at a given grid point x_i, $2 \leq i \leq M-3$, can be written as

$$u_{x,i}^+ = -\frac{1}{12}\frac{\Delta^+ u_{i+1}}{h} + \frac{7}{12}\frac{\Delta^+ u_i}{h} + \frac{7}{12}\frac{\Delta^+ u_{i-1}}{h} - \frac{1}{12}\frac{\Delta^+ u_{i-2}}{h} + g\left(\frac{\Delta^-\Delta^+ u_{i+2}}{h}, \frac{\Delta^-\Delta^+ u_{i+1}}{h}, \frac{\Delta^-\Delta^+ u_i}{h}, \frac{\Delta^-\Delta^+ u_{i-1}}{h}\right), \tag{22}$$

where it is recalled that the function g is defined by expression (13) with (10) and (14).

Boundary treatment. Similar to the left-biased WENO approximation (12), the right-biased WENO approximation (22) is only valid for "interior" grid points sufficiently away from the boundary of the Cartesian grid $\partial\mathfrak{S}^h$, that is, now, grid points x_i with $2 \leq i \leq M-3$. Making use again of symmetry arguments, the right-biased WENO approximation at the "boundary" grid point x_0 can be readily determined to be given by the formula

$$u_{x,0}^+ = \frac{13}{3}\frac{\Delta^+ u_1}{h} - \frac{31}{6}\frac{\Delta^+ u_2}{h} + \frac{11}{6}\frac{\Delta^+ u_3}{h} - g_0\left(\frac{\Delta^-\Delta^+ u_1}{h}, \frac{\Delta^-\Delta^+ u_2}{h}, \frac{\Delta^-\Delta^+ u_3}{h}, \frac{\Delta^-\Delta^+ u_4}{h}\right),$$

where we recall that the function g_0 is given by expression (20) with (18) and (21). The corresponding right-biased WENO approximations for the remaining "boundary" grid points x_1, x_{M-2}, x_{M-1}, and x_M are recorded in Appendix A.

Alternative boundary treatments. At this point, it is fitting to mention that alternative schemes for the left-biased and right-biased WENO approximations for the "boundary" grid points could also be employed. For instance, a WENO-type extrapolation could be used to estimate the value of the function $u(x)$ at ghost points located *outside* of the computational domain in order to allow the subsequent use of the left-biased and right-biased approximations (12) and (22) at *all* grid points in the computational domain; see, e.g., [41]. If the function is expected to be smooth in the vicinity of the boundaries of the computational domain, a simpler Lagrange extrapolation of the value of the function $u(x)$ at some ghost points or directly of its first derivative at the grid points close to the boundaries could also be alternatively employed. As yet another possible approach, in the context of the HJ equation (1)–(2), the "space" derivatives at the boundaries could be obtained not from neighboring grid points as presented above, but directly from the "time" derivatives of the boundary conditions through the PDE $(1)_1$ itself; see, e.g., [42] and references therein. In this work, we favor the boundary treatment spelled out above because of its overall mathematical consistency with the WENO approximation utilized for the "interior" grid points.

3.1.2. WENO approximation of the first partial derivatives of a multivariable function

The left-biased and right-biased fifth-order WENO approximations of the first *partial* derivatives of a multivariable function $u(x^{(1)}, x^{(2)}, \ldots, x^{(d)})$ can now be readily generated by repeatedly using the one-dimension procedure laid out in the previous subsection in a dimension-by-dimension fashion for each variable $x^{(1)}, x^{(2)}, \ldots, x^{(d)}$. For clarity of presentation, we spell out these approximations for a function of two variables $u(x, y)$, where for further clarity we employ the variables (x, y) instead of $(x^{(1)}, x^{(2)})$. Consistent with this notation, we denote by (x_i, y_j) the coordinates of the (i, j) vertex in the Cartesian grid $\mathfrak{S}^h = \{(x_i, y_j) : x_i = x_0 + ih_x, y_j = y_0 + jh_y, 0 \leq i \leq M_x, 0 \leq j \leq M_y\}$ comprising $M_x + 1$ ($M_y + 1$) vertices uniformly spaced by h_x (h_y) in the x-(y-)direction. The left-biased WENO approximations of the partial derivatives $\partial u(x_i, y_j)/\partial x$ and $\partial u(x_i, y_j)/\partial y$ are then given, respectively, by the formulas

$$u_{x,i,j}^- = -\frac{1}{12}\frac{\Delta_x^+ u_{i-2,j}}{h_x} + \frac{7}{12}\frac{\Delta_x^+ u_{i-1,j}}{h_x} + \frac{7}{12}\frac{\Delta_x^+ u_{i,j}}{h_x} - \frac{1}{12}\frac{\Delta_x^+ u_{i+1,j}}{h_x} - g\left(\frac{\Delta_x^-\Delta_x^+ u_{i-2,j}}{h_x}, \frac{\Delta_x^-\Delta_x^+ u_{i-1,j}}{h_x}, \frac{\Delta_x^-\Delta_x^+ u_{i,j}}{h_x}, \frac{\Delta_x^-\Delta_x^+ u_{i+1,j}}{h_x}\right), \quad 3 \leq i \leq M_x - 2,\ 0 \leq j \leq M_y, \tag{23}$$

$$u^{-}_{y,i,j} = -\frac{1}{12}\frac{\Delta^{+}_{y}u_{i,j-2}}{h_y} + \frac{7}{12}\frac{\Delta^{+}_{y}u_{i,j-1}}{h_y} + \frac{7}{12}\frac{\Delta^{+}_{y}u_{i,j}}{h_y} - \frac{1}{12}\frac{\Delta^{+}_{y}u_{i,j+1}}{h_y} - g\left(\frac{\Delta^{-}_{y}\Delta^{+}_{y}u_{i,j-2}}{h_y}, \frac{\Delta^{-}_{y}\Delta^{+}_{y}u_{i,j-1}}{h_y}, \frac{\Delta^{-}_{y}\Delta^{+}_{y}u_{i,j}}{h_y}, \frac{\Delta^{-}_{y}\Delta^{+}_{y}u_{i,j+1}}{h_y}\right), \quad 0 \le i \le M_x,\ 3 \le j \le M_y - 2. \tag{24}$$

Similarly, the right-biased WENO approximations of the partial derivatives $\partial u(x_i, y_j)/\partial x$ and $\partial u(x_i, y_j)/\partial y$ are then given by

$$u^{+}_{x,i,j} = -\frac{1}{12}\frac{\Delta^{+}_{x}u_{i+1,j}}{h_x} + \frac{7}{12}\frac{\Delta^{+}_{x}u_{i,j}}{h_x} + \frac{7}{12}\frac{\Delta^{+}_{x}u_{i-1,j}}{h_x} - \frac{1}{12}\frac{\Delta^{+}_{x}u_{i-2,j}}{h_x} + g\left(\frac{\Delta^{-}_{x}\Delta^{+}_{x}u_{i+2,j}}{h_x}, \frac{\Delta^{-}_{x}\Delta^{+}_{x}u_{i+1,j}}{h_x}, \frac{\Delta^{-}_{x}\Delta^{+}_{x}u_{i,j}}{h_x}, \frac{\Delta^{-}_{x}\Delta^{+}_{x}u_{i-1,j}}{h_x}\right), \quad 2 \le i \le M_x - 3,\ 0 \le j \le M_y, \tag{25}$$

$$u^{+}_{y,i,j} = -\frac{1}{12}\frac{\Delta^{+}_{y}u_{i,j+1}}{h_y} + \frac{7}{12}\frac{\Delta^{+}_{y}u_{i,j}}{h_y} + \frac{7}{12}\frac{\Delta^{+}_{y}u_{i,j-1}}{h_y} - \frac{1}{12}\frac{\Delta^{+}_{y}u_{i,j-2}}{h_y} + g\left(\frac{\Delta^{-}_{y}\Delta^{+}_{y}u_{i,j+2}}{h_y}, \frac{\Delta^{-}_{y}\Delta^{+}_{y}u_{i,j+1}}{h_y}, \frac{\Delta^{-}_{y}\Delta^{+}_{y}u_{i,j}}{h_y}, \frac{\Delta^{-}_{y}\Delta^{+}_{y}u_{i,j-1}}{h_y}\right), \quad 0 \le i \le M_x,\ 2 \le j \le M_y - 3, \tag{26}$$

respectively, where, in complete analogy with the notation employed in the single-variable case, $\Delta^{+}_{x}v_{i,j} = v_{i+1,j} - v_{i,j}$, $\Delta^{-}_{x}v_{i,j} = v_{i,j} - v_{i-1,j}$, $\Delta^{+}_{y}v_{i,j} = v_{i,j+1} - v_{i,j}$, $\Delta^{-}_{y}v_{i,j} = v_{i,j} - v_{i,j-1}$, and where it is recalled that the function g is defined by expression (13) with (10) and (14). Note that the formulas (23) through (26) are valid only for "interior" grid points. The corresponding WENO approximations for "boundary" grid points should now be apparent, as well as the corresponding formulas for functions $u(x^{(1)}, x^{(2)}, \ldots, x^{(d)})$ of d variables.

3.2. The "space" discretization

Having introduced the left-biased and right-biased WENO approximations of interest here for the first partial derivatives of scalar-valued functions over arbitrary Cartesian grids of finite extent, we are now equipped to lay out the discretization of the HJ equation (1)–(2) in its "space" variables **F**, **E**, and **H**. For clarity of exposition, we shall limit the presentation to the case when the HJ equation (1)–(2) involves only two of their $N^2 + 2N$ "space" variables (F_{ij}, E_i, H_i, $i, j = 1, \ldots, N$). We denote those by x and y and, with a slight abuse of notation, write

$$\begin{cases} \dfrac{\partial W}{\partial \mathtt{c}} + \mathcal{H}\left(x, y, \mathtt{c}, W, \dfrac{\partial W}{\partial x}, \dfrac{\partial W}{\partial y}\right), & (x, y) \in \mathfrak{S}, \quad \mathtt{c} \in \mathfrak{T} \\ W(x, y, 1) = W_{\mathtt{i}}(x, y), & (x, y) \in \mathfrak{S} \end{cases}, \tag{27}$$

where the Hamiltonian $\mathcal{H}$ is given by the appropriate specialization of (2). The corresponding discretization of the general HJ equation (1)–(2) involving all $N^2 + 2N$ "space" variables will be apparent from this special case and thus will not be explicitly formulated.

In their celebrated contribution, Crandall and Lions [8] and Souganidis [43] proved that the so-called first-order monotone schemes converge to the viscosity solution of HJ equations with the refinement of the grid where the approximation in the "space" variables is generated. Our first step in the "space" discretization of (27) is thus to discretize the "space" domain $\mathfrak{S}$ into a Cartesian grid $\mathfrak{S}^h = \{(x_i, y_j) : x_i = x_0 + ih_x, y_j = y_0 + jh_y, 0 \le i \le M_x, 0 \le j \le M_y\}$ comprising $M_x + 1$ ($M_y + 1$) vertices uniformly spaced by h_x (h_y) in the x-(y-)direction; for subsequent expediency, we denote by $W_{i,j} = W_{i,j}(\mathtt{c})$ the sought after numerical approximation $W(x_i, y_j, \mathtt{c})$ of the viscosity solution of (27) at the "space" point $(x, y) = (x_i, y_j) \in \mathfrak{S}^h$ and "time" $\mathtt{c}$. In this context, first-order monotone schemes refer then to numerical schemes of the semi-discrete form

$$\begin{cases} \dfrac{\partial W_{i,j}}{\partial \mathtt{c}} = -\widehat{\mathcal{H}}\left(x_i, y_j, \mathtt{c}, W_{i,j}, \dfrac{\Delta^{+}_{x}W_{i,j}}{h_x}, \dfrac{\Delta^{-}_{x}W_{i,j}}{h_x}, \dfrac{\Delta^{+}_{y}W_{i,j}}{h_y}, \dfrac{\Delta^{-}_{y}W_{i,j}}{h_y}\right), & \mathtt{c} \in \mathfrak{T} \\ W_{i,j}(1) = W_{\mathtt{i}}(x_i, y_j) \end{cases}, \tag{28}$$

where the so-called numerical Hamiltonian $\widehat{\mathcal{H}}$ (also termed numerical flux) is any Lipschitz continuous function that is *consistent* with the Hamiltonian $\mathcal{H}$ in the sense that

$$\widehat{\mathcal{H}}(x, y, \mathsf{c}, W, p, p, q, q) = \mathcal{H}(x, y, \mathsf{c}, W, p, q),$$

and is *monotone* in the sense that it is nonincreasing in its fifth and seventh arguments and nondecreasing in its sixth and eighth arguments, symbolically,

$$\widehat{\mathcal{H}}(x, y, \mathsf{c}, W, \downarrow, \uparrow, \downarrow, \uparrow).$$

The above conditions on $\widehat{\mathcal{H}}$ ensure convergence of $W_{i,j}$ to the viscosity solution W of (27) in the limit as $h_x, h_y \to 0$.

Now, with the objective of formulating a scheme that is robust and capable of delivering high accuracy, the second and last step in the "space" discretization of (27) is to replace in the numerical Hamiltonian $\widehat{\mathcal{H}}$ in (28) the first-order approximations $\Delta_x^+ W_{i,j}/h_x$, $\Delta_x^- W_{i,j}/h_x$, $\Delta_y^+ W_{i,j}/h_y$, $\Delta_y^- W_{i,j}/h_y$ of the partial derivatives of W by higher-order approximations.[6] In particular, we replace these left-biased and right-biased first-order approximations with the corresponding left-biased and right-biased fifth-order WENO approximations presented in the previous subsection, as given, in the present case of two "space" variables x and y, by the expressions (23)–(26) for the "interior" grid points and by the corresponding extensions of the expressions reported in Appendix A for the "boundary" grid points.

The choice of numerical Hamiltonian $\widehat{\mathcal{H}}$. There is a number of monotone numerical Hamiltonians that have been proposed in the literature over the years; see, e.g., [44] and [45]. In this work, we make use of the so-called Roe flux with local Lax–Friedrich (LLF) entropy correction [44]. Omitting the explicit dependence on x, y, c, and W to ease notation, this numerical Hamiltonian reads as

$$\widehat{\mathcal{H}}(p^+, p^-, q^+, q^-) = \begin{cases} \mathcal{H}\left(p^*, q^*\right) & \text{if } \mathcal{H}_1(p,q) \text{ and } \mathcal{H}_2(p,q) \text{ do not change signs in } p \in I(p^-, p^+), q \in I(q^-, q^+); \\ \mathcal{H}\left(\dfrac{p^+ + p^-}{2}, q^*\right) - \nu_1(p^+, p^-)\dfrac{p^+ - p^-}{2} & \text{otherwise and if } \mathcal{H}_2(p,q) \text{ does not change sign in } A \le p \le B, q \in I(q^-, q^+); \\ \mathcal{H}\left(p^*, \dfrac{q^+ + q^-}{2}\right) - \nu_2(q^+, q^-)\dfrac{q^+ - q^-}{2} & \text{otherwise and if } \mathcal{H}_1(p,q) \text{ does not change sign in } p \in I(p^-, p^+), C \le q \le D; \\ \widehat{\mathcal{H}}^{LLF}\left(p^+, p^-, q^+, q^-\right) & \text{otherwise} \end{cases} \tag{29}$$

where p^* and q^* are defined by

$$p^* = \begin{cases} p^+ & \text{if } \mathcal{H}_1(p,q) \le 0 \\ p^- & \text{if } \mathcal{H}_1(p,q) \ge 0 \end{cases}, \qquad q^* = \begin{cases} q^+ & \text{if } \mathcal{H}_2(p,q) \le 0 \\ q^- & \text{if } \mathcal{H}_2(p,q) \ge 0 \end{cases},$$

ν_1 and ν_2 are defined by

$$\nu_1(p^+, p^-) = \max_{\substack{p \in I(p^-, p^+) \\ C \le q \le D}} |\mathcal{H}_1(p,q)|, \qquad \nu_2(q^+, q^-) = \max_{\substack{q \in I(q^-, q^+) \\ A \le p \le B}} |\mathcal{H}_2(p,q)|,$$

and

$$\widehat{\mathcal{H}}^{LLF}\left(p^+, p^-, q^+, q^-\right) = \mathcal{H}\left(\frac{p^+ + p^-}{2}, \frac{q^+ + q^-}{2}\right) - \nu_1(p^+, p^-)\frac{p^+ - p^-}{2} - \nu_2(q^+, q^-)\frac{q^+ - q^-}{2}.$$

In the above expressions, $\mathcal{H}_1 = \partial\mathcal{H}(p,q)/\partial p$, $\mathcal{H}_2 = \partial\mathcal{H}(p,q)/\partial q$, $[A, B]$ ($[C, D]$) denotes the range of values taken by $p^\pm$ ($q^\pm$) over the entire "space" (x, y) considered, and $I(a,b) = [\min(a,b), \max(a,b)]$. The rationale behind this choice of numerical Hamiltonian is threefold. It has been successfully utilized in a variety of hyperbolic conservation laws and HJ equations alike and exhibits fairly low numerical dissipation (see, e.g., Chapter 5 in [4]). Further, its implementation for any number of "space" variables in a computer code is fairly straightforward.

[6] While the approach, originally introduced by Osher and Sethian [9], of replacing the first-order approximations of the "space" partial derivatives in (28) by higher-order approximations is yet to be shown *rigorously* to lead to schemes that are convergent to the viscosity solution, it has been repeatedly shown *numerically* to do just so.

3.3. The "time" discretization

The final step in the construction of the numerical scheme is to carry out the discretization of the semi-discrete HJ equation (28) in the "time" variable c. Based on an initial assessment of a plurality of explicit and implicit "time" integration methods, we select in this work a fifth-order explicit Runge–Kutta scheme due to Lawson [46]. The reasons behind this choice are that this method proved to remain stable and accurate over very long "times" in all of our numerical experiments, while, at the same time, it also outperformed in terms of computational cost all of the various implicit methods that we examined.

We thus proceed with the "time" discretization of (28) by first discretizing the "time" domain $\mathfrak{T}$ into a Cartesian grid $\mathfrak{T}^\delta = \{\mathsf{c}^k : \mathsf{c}^k = 1 - k\delta,\ 1 \le k \le T,\ T\delta = c\}$ with a constant "time" increment $\Delta\mathsf{c} = \delta$. We denote by $W^k_{i,j}$ the numerical approximation of the solution $W_{i,j}(\mathsf{c}^k)$ of (28) at the "space" point $(x, y) = (x_i, y_j) \in \mathfrak{S}^h$ and "time" $\mathsf{c} = \mathsf{c}^k \in \mathfrak{T}^\delta$. The next step is to lay out an algorithm to compute $W^{k+1}_{i,j}$ in terms of $W^k_{i,j}$ using appropriate estimates $W^{(l)}_{i,j}$ of the solution at certain intermediate "times" between c^k and c^{k+1}. To this end, it proves helpful to introduce the notation

$$L^{(l)}_{i,j}\{\mathsf{c}\} = -\widehat{\mathcal{H}}\left(x_i, y_j, \mathsf{c}, W^{(l)}_{i,j}, W^{(l)+}_{x,i,j}, W^{(l)-}_{x,i,j}, W^{(l)+}_{y,i,j}, W^{(l)-}_{y,i,j}\right), \tag{30}$$

where we emphasize that the numerical Hamiltonian $\widehat{\mathcal{H}}$ is given by the Roe flux (29) and that $W^{(l)\pm}_{x,i,j}$, $W^{(l)\pm}_{y,i,j}$ stand for the fifth-order WENO approximations of the partial derivatives of $W^{(l)}_{i,j}$ worked out in Section 3.1. Then, for the specific choice of fifth-order Runge–Kutta scheme summoned here, the solution $W^{k+1}_{i,j}$ is given in terms of $W^k_{i,j}$ by following the procedure

$$\begin{aligned}
&W^{(1)}_{i,j} = W^k_{i,j}, \qquad k^{(1)}_{i,j} = L^{(1)}_{i,j}\left\{\mathsf{c}^k\right\},\\
&W^{(2)}_{i,j} = W^{(1)}_{i,j} + \frac{1}{2}\Delta\mathsf{c}k^{(1)}_{i,j}, \qquad k^{(2)}_{i,j} = L^{(2)}_{i,j}\left\{\mathsf{c}^k + \frac{1}{2}\Delta\mathsf{c}\right\},\\
&W^{(3)}_{i,j} = W^{(1)}_{i,j} + \frac{1}{16}\Delta\mathsf{c}(3k^{(1)}_{i,j} + k^{(2)}_{i,j}), \qquad k^{(3)}_{i,j} = L^{(3)}_{i,j}\left\{\mathsf{c}^k + \frac{1}{4}\Delta\mathsf{c}\right\}\\
&W^{(4)}_{i,j} = W^{(1)}_{i,j} + \frac{1}{2}\Delta\mathsf{c}k^{(3)}_{i,j}, \qquad k^{(4)}_{i,j} = L^{(4)}_{i,j}\left\{\mathsf{c}^k + \frac{1}{2}\Delta\mathsf{c}\right\},\\
&W^{(5)}_{i,j} = W^{(1)}_{i,j} + \frac{3}{16}\Delta\mathsf{c}(-k^{(2)}_{i,j} + 2k^{(3)}_{i,j} + 3k^{(4)}_{i,j}), \qquad k^{(5)}_{i,j} = L^{(5)}_{i,j}\left\{\mathsf{c}^k + \frac{3}{4}\Delta\mathsf{c}\right\},\\
&W^{(6)}_{i,j} = W^{(1)}_{i,j} + \frac{1}{7}\Delta\mathsf{c}(k^{(1)}_{i,j} + 4k^{(2)}_{i,j} + 6k^{(3)}_{i,j} - 12k^{(4)}_{i,j} + 8k^{(5)}_{i,j}), \qquad k^{(6)}_{i,j} = L^{(6)}_{i,j}\left\{\mathsf{c}^k + \Delta\mathsf{c}\right\},\\
&W^{k+1}_{i,j} = W^k_{i,j} + \frac{1}{90}\Delta\mathsf{c}\left(7k^{(1)}_{i,j} + 32k^{(3)}_{i,j} + 12k^{(4)}_{i,j} + 32k^{(5)}_{i,j} + 7k^{(6)}_{i,j}\right).
\end{aligned} \tag{31}$$

It is plain from this sequential set of steps that this is an *explicit* integration scheme, that is, $W^{k+1}_{i,j}$ is computed from knowledge $W^k_{i,j}$ via the sequential *evaluations* of the quantities $k^{(l)}_{i,j}$, $1 \le l \le 6$. From an implementation point of view it is thus simple and efficient. Theoretically, it has the merit to exhibit an extended region of stability when applied to linear differential equations of the form $\mathrm{d}u(t)/\mathrm{d}t = \lambda u(t),\ \lambda \in \mathbb{C}$; see [46]. Moreover, within the related context of hyperbolic conservation laws, the integration scheme (31) has the further merit to be strong stability preserving (SSP) under the Courant–Friedrichs–Levy (CFL) condition

$$|\Delta\mathsf{c}| \le \frac{7}{30}|\Delta\mathsf{c}_{FE}|$$

if the first-order forward and backward Euler time discretizations $W^{k+1}_{i,j} = W^k_{i,j} \pm \Delta\mathsf{c}L^k_{i,j}\left\{\mathsf{c}^k\right\}$ are SSP under the CFL condition

$$|\Delta\mathsf{c}| \le |\Delta\mathsf{c}_{FE}|;$$

see Section II in [47] and Lemma 2.2 in [48]. This latter feature suggests the heuristic CFL condition

$$|\Delta \mathtt{c}| \max\left\{\frac{|\mathcal{H}_1(p,q)|}{h_x}+\frac{|\mathcal{H}_2(p,q)|}{h_y}\right\} \leq \frac{7}{30} \tag{32}$$

for the Runge–Kutta time discretization (31) of the semi-discrete HJ equation (28) under investigation here; see, e.g., Chapter 5 in [4]. In practice, we make use of a different CFL condition, which is discussed in the next subsection. Finally, we note that the corresponding "time" discretization of the semi-discrete form (28) resulting from the general HJ equation (1)–(2) involving all N^2+2N "space" variables immediately follows from the corresponding trivial extension of the numerical Hamiltonian in (30).

3.4. The scheme

The whole of the scheme laid out in the three preceding subsections can be readily implemented into a computer code and deployed to efficiently generate accurate approximations for the viscosity solution W of the HJ equation (1)–(2). In the sequel, we walk through the entire algorithmic process and make a number of important practical remarks on its implementation along the way.

The specification of the composite material of interest. The first step in the algorithmic process of the scheme is, of course, the selection of specific free-energy functions $W_{\mathtt{m}}$ and $W_{\mathtt{i}}$ describing the magneto-electro-elastic behaviors of the underlying matrix and inclusions, and of the volume fraction c and two-point correlation $p_0^{(\mathtt{ii})}(\mathbf{X})$ describing the content, shape, and spatial arrangement of inclusions.

The choice of "space" discretization. The second step is the selection of a specific discretization $\mathfrak{S}^h$ of the "space" domain $\mathfrak{S}$ describing the range of deformation gradient tensors $\mathbf{F}$, electric fields $\mathbf{E}$, and magnetic fields $\mathbf{H}$ of interest for the problem at hand. In general, it suffices to employ the same grid spacing h for all the "space" variables involved.

More critically, since $\mathfrak{S}^h$ is necessarily of *finite* extent, one has to examine each part of its boundary $\partial\mathfrak{S}^h$ to check whether characteristics "enter" or "exit" through them. For the "space" discretized problem to be well posed, the value of the sought-after function W must be *prescribed* as a boundary condition on the parts of the boundary $\partial\mathfrak{S}^h$ where the characteristics "enter" the domain of computation, while no boundary data needs to be prescribed on the complementary parts of $\partial\mathfrak{S}^h$ where the characteristics "exit" $\mathfrak{S}^h$; see, e.g., Chapter 8 in [49] and Chapter 10 in [39] for a general discussion of this important point. Since the viscosity solution W of the HJ equation (1)–(2) is expected to be at least twice continuously differentiable, we propose to carry out the identification and computation of such "inflow" boundary conditions on $\partial\mathfrak{S}^h$ via the method of characteristics. We provide the relevant details in Appendix B.

Another important point that can affect the specific selection of "space" discretization is that, because of the choice of matrix and inclusion free-energy functions $W_{\mathtt{m}}$ and $W_{\mathtt{i}}$, the viscosity solution W of the HJ equation (1)–(2) may satisfy certain constraints in the sense that it may become unbounded (from above and/or from below) at certain sets of *known* finite values of $\mathbf{F}$, $\mathbf{E}$, and/or $\mathbf{H}$. These sets may not be conforming with the Cartesian grids that we employ here for $\mathfrak{S}^h$, and hence they may be difficult to resolve numerically. One straightforward way to resolve this problem[7] is to identify an appropriate change of "space" variables $\mathbf{F}$, $\mathbf{E}$, and/or $\mathbf{H}$ so as to "straighten" the "curved" boundaries associated with the constraints, and carry out the "space" discretization of (1)–(2) in those new "space" variables. An example of this is presented in the next section.

The choice of "time" discretization. The third step in the algorithm process is the selection of a specific discretization $\mathfrak{T}^\delta$ of the "time" domain $\mathfrak{T}$ and, by the same token, a specific CFL condition. In this regard, we remark that the Hamiltonian (2) depends explicitly on the "time" variable $\mathtt{c}$ through the common multiplicative factor of $1/\mathtt{c}$. This dependence causes a severe computational problem of convergence when constructing approximations of viscosity solutions W featuring small-to-moderate volume fractions of inclusions, partly because it effectively forces the "time" increments $\Delta\mathtt{c}$ to be proportional to the "time" $\mathtt{c}$ itself. A simple approach that circumvents this issue is to make use of the change of "time" variable $\mathtt{t}=-\ln\mathtt{c}$, under which the resulting HJ equation (1)–(2) no longer depends explicitly on "time". Under this change of variable we also note that the "time" domain $\mathfrak{T}$ takes

[7] Alternatively, one could use simplicial meshes; see, e.g., [50].

the more standard form $\mathfrak{T} = (0, t]$ with $t = -\ln c$. Furthermore, our numerical experiments for a variety of cases indicate that in terms of the "time" variable $\mathtt{t}$ a simple constant CFL condition, typically in the range

$$\frac{1}{50} \leq \frac{\Delta \mathtt{t}}{h} \leq 1,$$

suffices to achieve optical convergence rates. For these reasons, in practice, we favor the use of $\mathtt{t}$ instead of $\mathtt{c}$ as the "time" variable.

In summary, for given choices of material and microstructure inputs, $W_{\mathtt{m}}$, $W_{\mathtt{i}}$, c, $p_0^{(\mathtt{ii})}(\mathbf{X})$, and given choices of "space" and "time" discretizations, $\mathfrak{S}^h$ and $\mathfrak{T}^\delta$, the approximation of the viscosity solution W is constructed at "space" grid points in $\mathfrak{S}^h$, all at once, starting at the initial "time" $\mathtt{t} = -\ln 1 = 0$, when $W = W_{\mathtt{i}}$, and progressing in "time" along the grid points in $\mathfrak{T}^\delta$ by following the (appropriate extended version of the) integration procedure (31) until the desired volume fraction of inclusions c, as parametrized by $t = -\ln c$, is reached.

4. Accuracy and convergence assessment

By construction, the scheme proposed in the preceding section is expected to be accurate and feature a high-order rate of convergence, specifically, an overall rate of convergence between third and fifth order, depending on the gradients exhibited by the solution W in its "space" variables $\mathbf{F}$, $\mathbf{E}$, and $\mathbf{H}$. In this section, we assess this expectation by investigating the actual performance of the scheme. We do so by directly confronting the numerical solution generated by the scheme with a simple explicit solution available for the HJ equation (1)–(2) for the case when it takes the particular form [23]

$$\begin{cases} \dfrac{\partial W}{\partial \mathtt{c}} + \mathcal{H}\left(\lambda_1, \lambda_2, \mathtt{c}, W, \dfrac{\partial W}{\partial \lambda_1}, \dfrac{\partial W}{\partial \lambda_2}\right) = 0, \quad (\lambda_1, \lambda_2) \in \mathfrak{S}, \quad \mathtt{c} \in \mathfrak{T} \\ W(\lambda_1, \lambda_2, 1) = 0, \quad (\lambda_1, \lambda_2) \in \mathfrak{S} \end{cases}, \tag{33}$$

where $\mathfrak{S} = \{\lambda_1 \in \mathbb{R}^+, \lambda_2 \in \mathbb{R}^+ : \lambda_1\lambda_2 > 1 - c\}$ and $\mathfrak{T} = [c, 1)$, with Hamiltonian

$$\mathcal{H} = -\frac{1}{\mathtt{c}} W + \frac{2 + \lambda_1\lambda_2\left(\lambda_1^2 + \lambda_2^2 - 4\right)}{4\mathtt{c}\lambda_1\lambda_2} G + \frac{\lambda_1^2 + \lambda_1\lambda_2 - 2}{2\mathtt{c}(\lambda_1 + \lambda_2)} \frac{\partial W}{\partial \lambda_1} + \frac{\lambda_2^2 + \lambda_1\lambda_2 - 2}{2\mathtt{c}(\lambda_1 + \lambda_2)} \frac{\partial W}{\partial \lambda_2} +$$

$$\frac{\lambda_1\lambda_2}{2\mathtt{c}G(\lambda_1 + \lambda_2)^2} \left(\frac{\partial W}{\partial \lambda_1}\right)\left(\frac{\partial W}{\partial \lambda_2}\right) - \frac{\lambda_1^2}{4\mathtt{c}G(\lambda_1 + \lambda_2)^2} \left(\frac{\partial W}{\partial \lambda_1}\right)^2 - \frac{\lambda_2^2}{4\mathtt{c}G(\lambda_1 + \lambda_2)^2} \left(\frac{\partial W}{\partial \lambda_2}\right)^2. \tag{34}$$

The HJ equation (33)–(34) corresponds to the specialization of the general HJ equation (1)–(2) to the $N = 2$ dimensional case when the applied deformation gradient, electric field, and magnetic field are set to

$$\mathbf{F} = \mathrm{diag}(\lambda_1, \lambda_2), \qquad \mathbf{E} = \mathbf{0}, \qquad \mathbf{H} = \mathbf{0},$$

the constitutive behavior of the matrix material is characterized by the Neo-Hookean stored-energy function

$$W_{\mathtt{m}}(\mathbf{F}, \mathbf{0}, \mathbf{0}) = \begin{cases} \dfrac{G}{2}\left[\mathbf{F} \cdot \mathbf{F} - 2\right] & \text{if} \quad \det \mathbf{F} = 1 \\ +\infty & \text{otherwise} \end{cases},$$

with G denoting its initial shear modulus, the inclusions are vacuous, so that $W_{\mathtt{i}}(\mathbf{F}, \mathbf{0}, \mathbf{0}) = 0$, their initial volume fraction is c and their spatial distribution is isotropic, so that $\nu(\boldsymbol{\xi}) = 1/2\pi$. Physically, the viscosity solution W of (33)–(34) corresponds hence to the homogenized free energy that characterizes the macroscopic elastic response of an isotropic porous elastomer comprised of Gaussian rubber embedding an isotropic distribution of closed-cell vacuous pores with initial volume fraction, or initial porosity, c. Fig. 1 shows a schematic of this physical significance with the various quantities of interest indicated. From a mathematical point of view, we should also remark that the "space" domain $\mathfrak{S}$ in (33) is semi-unbounded and features a "curved" boundary, namely, $\lambda_1\lambda_2 = 1 - c$, at which $W = +\infty$. This is nothing more than the manifestation of the fact that the current porosity in any deforming porous elastomer with incompressible elastomeric matrix vanishes, that is, complete closure of the underlying pores ensues, whenever the determinant of the macroscopic deformation gradient $\mathbf{F}$ reaches the critical value $\det \mathbf{F} = 1 - c$, at which point the porous elastomer behaves as an incompressible solid for loadings with any

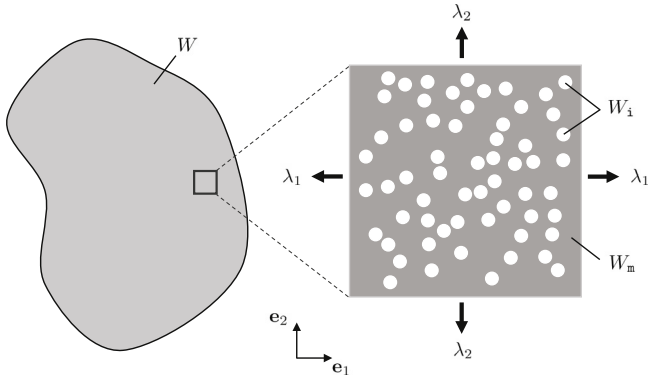

Fig. 1. Schematic representation of the physical meaning of the viscosity solution W of the HJ equation (33)–(34).

further volumetric compression; see, e.g., Sections 2 and 4.1 in [25].

The exact analytical solution. In spite of its strong nonlinearity and of the full dependence on the Hamiltonian (34) on the "space" variables λ_1, λ_2, the "space" derivatives $\partial W/\partial\lambda_1$, $\partial W/\partial\lambda_2$, the "time" variable $\mathtt{c}$, and on the solution W itself, the viscosity solution of the HJ equation (33)–(34) can be worked out in a simple closed form for any value of initial volume fraction of pores $c \in (0, 1]$. The result reads as [23]

$$W(\lambda_1, \lambda_2, c) = \frac{G}{2}\frac{1-c}{1+c}\left[\lambda_1^2 + \lambda_2^2 - 2\right] + \frac{G}{2}(\lambda_1\lambda_2 - 1)\left[\ln\left(\frac{\lambda_1\lambda_2 + c - 1}{c\lambda_1\lambda_2}\right) - 2\frac{1-c}{1+c}\right]. \tag{35}$$

4.1. An expedient change of variables

In preparation to construct the WENO finite-difference solution of (33)–(34) and compare it with the exact solution (35), as pointed out in Section 3.4, it is convenient first to make a change of "space" variables to straighten the "curved" boundary $\lambda_1\lambda_2 = 1 - c$ in the "space" domain $\mathfrak{S}$ so as to make it conforming with any Cartesian grid selected for the discretized "space" domain $\mathfrak{S}^h$. Likewise, it is convenient to make a change of "time" variable to circumvent dealing with the numerical problems associated with the factor $1/\mathtt{c}$ in the Hamiltonian (34). Accordingly, for definiteness and consistency between the "space" and "time" variables, we shall make use of the following change of variables:

$$x = \ln\left(\frac{\lambda_1}{\lambda_2}\right), \quad y = \ln(\lambda_1\lambda_2), \quad \text{and} \quad \mathtt{t} = -\ln \mathtt{c}.$$

In this new set of "space" and "time" variables, the HJ equation (33)–(34) takes the form

$$\begin{cases} \dfrac{\partial W}{\partial \mathtt{t}} + \mathcal{H}\left(x, y, W, \dfrac{\partial W}{\partial x}, \dfrac{\partial W}{\partial y}\right) = 0, \quad (x, y) \in \mathfrak{S}, \quad \mathtt{t} \in \mathfrak{T} \\ W(x, y, 0) = 0, \quad (x, y) \in \mathfrak{S} \end{cases} \tag{36}$$

where now $\mathfrak{S} = \{x \in \mathbb{R}, y \in \mathbb{R} : y > \ln(1 - e^{-t})\}$ and $\mathfrak{T} = (0, t]$, with Hamiltonian

$$\mathcal{H} = W - \frac{G}{2}\left[e^y \cosh x + e^{-y} - 2\right] - e^{-y}\tanh\left(\frac{x}{2}\right)\frac{\partial W}{\partial x} - \left[1 - e^{-y}\right]\frac{\partial W}{\partial y} + \frac{e^{-y}}{4G\cosh^2(x/2)}\left(\frac{\partial W}{\partial x}\right)^2; \tag{37}$$

in this expression, with a slight abuse of notation, we still write $W = W(x, y, \mathtt{t})$ and recall that $t = -\ln c$. Furthermore, in this new set of variables, the viscosity solution (35) reads as

$$W(x, y, t) = 2Ge^y \sinh^2\left(\frac{x}{2}\right)\tanh\left(\frac{t}{2}\right) + \frac{G}{2}\left(e^y - 1\right)\ln\left(e^{-y} + e^t - e^{t-y}\right). \tag{38}$$

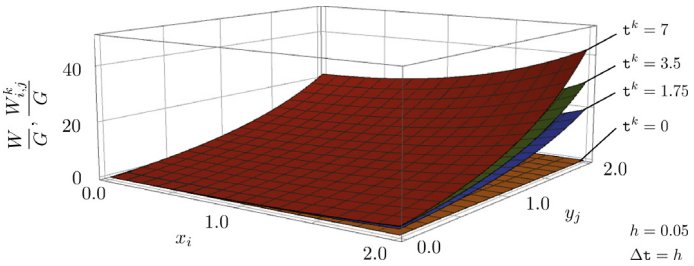

Fig. 2. Comparisons between the WENO finite-difference solution $W^k_{i,j}$ and the exact solution W for the HJ equation (36)–(37) at four different "times", $\mathfrak{t}^k = 0, 1.75, 3.5, 7$.

4.2. The WENO finite-difference solution

We now proceed with the construction of the WENO finite-difference solution for the HJ equation (36)–(37). For definiteness,[8] we consider the following computational domains

$$\mathfrak{S}^h = \{(x_i, y_j) : x_i = ih, y_j = jh, 0 \le i \le M, 0 \le j \le M, Mh = 2\} \tag{39}$$

and

$$\mathfrak{T}^\delta = \{\mathfrak{t}^k : \mathfrak{t}^k = k\Delta\mathfrak{t}, 1 \le k \le T, T\Delta\mathfrak{t} = 7\}.$$

Physically, these correspond to stretches in the set $\{\lambda_1 \in \mathbb{R}^+, \lambda_2 \in \mathbb{R}^+ : 1 \le \lambda_1/\lambda_2 \le 7.38, 1 \le \lambda_1\lambda_2 \le 7.38\}$ and to initial volume fractions of pores in the range $c \in [0.001, 1)$.

Granted the above specific selection of "space" discretization (39), as elaborated in Section 3.4, the next step is to identify the parts of its boundary where the value of the function W needs to be prescribed in order to render a well-posed discrete problem. To avoid loss of continuity, the relevant calculations are presented in Appendix B. With those results at hand, the rest of the implementation of the scheme continues to follow the steps outlined in the preceding section. In these, we note that the heuristic result (32) suggests the use of the CFL condition $\Delta\mathfrak{t} \le 0.15h$. However, numerical experiments indicate that the choice of "time" increment $\Delta\mathfrak{t} = h$ yields appropriate numerical solutions and, moreover, that "time" increments smaller than $\Delta\mathfrak{t} = h$ do not lead to additional accuracy for a given grid size h. Accordingly, all the results that are reported below correspond to computations with the CFL condition $\Delta\mathfrak{t} = h$.

We begin by examining the accuracy of the scheme in a qualitative manner. Fig. 2 shows comparisons between the exact solution W given by (38) and the numerical solution $W^k_{i,j}$ generated by the proposed scheme over the entire discretized "space" domain (39) for the relatively coarse grid size $h = 0.05$; recall that $\Delta\mathfrak{t} = h$. The solutions are presented normalized by the initial shear modulus G of the matrix material in terms of the "space" variables x and y for four different values of "time", $\mathfrak{t}^k = 0, 1.75, 3.5, 7$. The main observation from this figure is that the numerical solution is virtually indistinguishable from the exact one for all considered "times", which points to the accuracy of the proposed scheme.

In order to gain more precise quantitative insight into the accuracy and convergence properties of the scheme, we compute $e^k_{1,h}$ and $e^k_{\infty,h}$, the global relative errors in the discrete L^1 and L^∞ norms between the exact solution W, again, given by (38), and the numerical solution $W^k_{i,j}$ at the discrete time $\mathfrak{t}^k$ and for a given grid size h. They are defined by

$$e^k_{1,h} = \frac{\|W^k_{i,j} - W(x_i, y_j, \mathfrak{t}^k)\|_1}{\|W(x_i, y_j, \mathfrak{t}^k)\|_1} \quad \text{and} \quad e^k_{\infty,h} = \frac{\|W^k_{i,j} - W(x_i, y_j, \mathfrak{t}^k)\|_\infty}{\|W(x_i, y_j, \mathfrak{t}^k)\|_\infty}$$

in terms of the discrete norms

$$\|u^k_{i,j}\|_1 = h^2 \sum_{i,j=0}^{M} |u^k_{i,j}| \quad \text{and} \quad \|u^k_{i,j}\|_\infty = \max_{0 \le i,j \le M} |u^k_{i,j}|.$$

[8] We emphasize that in addition to the results reported here on the computational domain (39) we have generated analogous results on a number of different discretized "space" domains $\mathfrak{S}^h$, all of which exhibit the same accuracy and convergence properties.

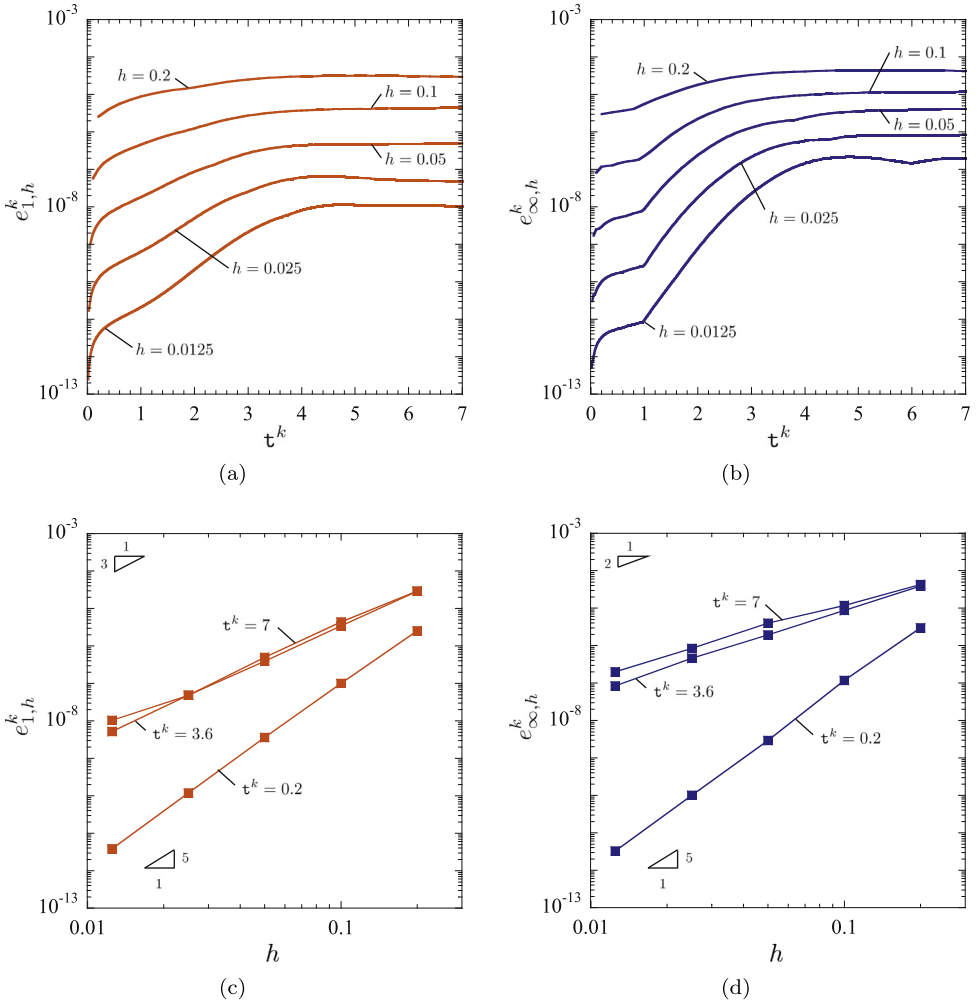

Fig. 3. Global error measures $e^k_{1,h}$ and $e^k_{\infty,h}$ between the numerical solution of the HJ equation (36)–(37) generated by the proposed scheme and the exact solution. The results are plotted as functions of: (a)–(b) the "time" $\mathtt{t}^k$ for fixed grid spacings $h = 0.2, 0.1, 0.05, 0.025, 0.0125$, and (c)–(d) the grid spacing h for fixed "times" $\mathtt{t}^k = 0.2, 3.6, 7$.

These error measures are plotted in Fig. 3(a)–(b) for fixed grid sizes $h = 0.2, 0.1, 0.05, 0.025, 0.0125$ at all times $\mathtt{t}^k \in \mathfrak{T}^\delta$. As already brought into view by Fig. 2, the values taken by $e^k_{1,h}$ and $e^k_{\infty,h}$, namely, $e^k_{1,h} \leq 3.0 \times 10^{-5}$ and $e^k_{\infty,h} \leq 4.0 \times 10^{-5}$, for all the grids considered confirm that the proposed scheme does indeed generate accurate numerical solutions. More specifically, for a given grid size h, both errors increase monotonically up to $\mathtt{t}^k \approx 4.0$ before leveling off or, in some cases, slightly decreasing for larger "times". On the other hand, for a given fixed "time" $\mathtt{t}^k$, both error measures decrease monotonically with the reduction of the grid size h. This point is better illustrated by Fig. 3(c)–(d), where $e^k_{1,h}$ and $e^k_{\infty,h}$ are plotted for the three fixed "times" $\mathtt{t}^k = 0.2, 3.6, 7$ as functions of h. Fig. 3(c)–(d) also reveal that both errors exhibit roughly a fifth-order rate of convergence, at least for small "times". For larger "times", the rate of convergence decreases to third order in the error measure $e^k_{1,h}$ and to second order in $e^k_{\infty,h}$. This decrease in the convergence rates might be the signature of the stiffness of the HJ equation (36)–(37); see, e.g., Chapters 6 and 7 in [51] for a general discussion on this topic. It might also be due to the presence of critical points along the boundary $x = 0$ where $\partial W(0, y, \mathtt{t})/\partial x = 0$; see [40]. Whatever the cause, the overall rate of convergence remains within the formally expected range.[9]

[9] Here, we should emphasize that when applied to simpler type of HJ equations, the proposed scheme does deliver an overall rate of convergence of fifth order for all "times". This was verified to be indeed the case for a number of HJ equations, such as for instance, the simple linear advection equation $\partial u/\partial t = \partial u/\partial x$ with $u(x, 0) = \sin(\pi x)$, $u(1, t) = \sin(\pi(1 + t))$ for $x \in [0, 1)$ and $t \in \mathbb{R}^+$.

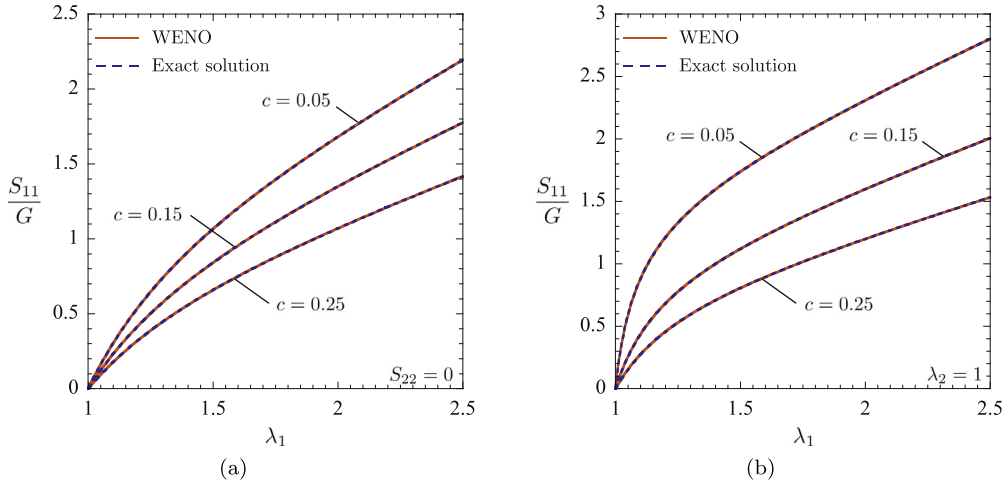

Fig. 4. Comparisons of the "space" derivative (physically, the first Piola–Kirchhoff stress) $S_{11} = \partial W/\partial \lambda_1$ computed from the proposed scheme (solid lines) and the corresponding exact solution (dashed lines) for two loading conditions: (a) uniaxial tension when $S_{22} = \partial W/\partial \lambda_2 = 0$ and (b) uniaxial stretch when $\lambda_2 = 1$. The results, which are normalized with respect to the initial shear modulus G of the matrix material, correspond to three different initial volume fractions of pores, $c = 0.05, 0.15, 0.25$, and are plotted in terms of the "space" variable (physically, the applied stretch) λ_1.

We close by reporting a further comparison between the "space" derivatives of W generated numerically by the proposed scheme and the corresponding exact solutions. As noted in remark i of Section 2, the first partial derivatives of W with respect to the original "space" variables $\mathbf{F}$, $\mathbf{E}$, $\mathbf{H}$ correspond to the constitutive relations (4) that describe the macroscopic response of the composite material at hand and hence are of primary importance for applications. In the present physical context of isotropic porous Gaussian elastomers, for definiteness, we consider the macroscopic stress–stretch response of the composite material under the following two loading conditions:

- Uniaxial tension when $S_{22} = \dfrac{\partial W}{\partial \lambda_2}(\lambda_1, \lambda_2, c) = 0$ with prescribed $\lambda_1 \geq 1$;
- Uniaxial stretch when $\lambda_2 = 1$ with prescribed $\lambda_1 \geq 1$.

Note that here we have reverted to the original – and therefore physical – "space" and "time" variables λ_1, λ_2, c. Fig. 4 shows comparisons between the "space" derivative $S_{11} = \partial W/\partial \lambda_1$ computed from the proposed scheme ($h = 0.05$, $\Delta \mathfrak{t} = h$) and the corresponding exact solution for the two loading conditions spelled out above. The results are presented for three different values of the initial volume fraction of pores, $c = 0.05, 0.15, 0.25$, as functions of the "space" variable λ_1. It is plain from both parts of the figure that the proposed scheme delivers accurate approximations not only for W but for its "space" derivatives as well.

5. Application to magnetorheological elastomers filled with ferrofluid inclusions

Having demonstrated the accuracy and convergence capabilities of the proposed scheme to generate solutions for the HJ equation (1)–(2), in this section, we showcase its potential to aid in the investigation of novel nonlinear and coupled phenomena. We do so by solving the boundary-value problem of a cylindrical specimen, made up of an elastomer filled with an isotropic distribution of ferrofluid inclusions, that, as in a typical experimental setup (see, e.g., [52,53]), is subjected to a remotely applied uniaxial magnetic field; see Fig. 5. To this end, the homogenized free-energy function W that characterizes the macroscopic magneto-elastic *material* response of the specimen is first generated numerically by solving the appropriate specialization of the HJ equation (1)–(2) via the proposed scheme. This numerical free energy is then utilized in the context of a macroscopic finite-element (FE) formulation[10] to solve for the deformation and magnetic fields within the cylindrical specimen and the surrounding air, which are

[10] Here, it is fitting to mention that some authors have recently proposed to investigate this same type of two-scale boundary-value problems with a FE^2 scheme; see, e.g., [54–56].

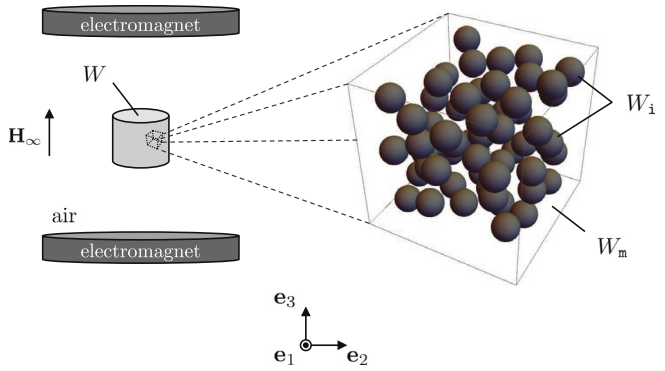

Fig. 5. Schematic of the boundary-value problem under investigation: a cylindrical specimen, made up of an elastomer filled with ferrofluid inclusions, is immersed in air and subjected to a remotely applied uniaxial magnetic field $\mathbf{H}_\infty$. The homogenized free-energy function W characterizing the macroscopic magneto-elastic material response of the specimen is determined by solving the appropriate specialization of the HJ equation (1)–(2) via the proposed WENO scheme. This numerical free energy is then used in a FE formulation to solve for the deformation and magnetic fields within the cylindrical specimen and surrounding air.

expected to be non-uniform [35,57]. In the sequel, we outline the basic details involved in the computation of W and report representative FE results for the macroscopic deformation and magnetic fields within the specimen. From a physical point of view, we remark that elastomers filled with ferrofluid inclusions constitute a new class of magnetorheological elastomers that has been recently identified in [35] as a promising pathway to circumvent the shortcomings of classical magnetorheological elastomers, in particular, elastomers filled with iron particles. Most notably, this new class of materials – as opposed to classical magnetorheological elastomers – can undergo relatively large deformations when exposed to a magnetic field of low intensity.

The WENO computation of the homogenized free energy W. To work out the appropriate specialization of the HJ equation (1)–(2), we begin by setting the dimension to $N = 3$ and the electric field to $\mathbf{E} = \mathbf{0}$. We model the matrix material as Gaussian rubber so that

$$W_\mathrm{m}(\mathbf{F},\mathbf{0},\mathbf{H}) = \begin{cases} \dfrac{G}{2}[\,I_1 - 3] - \dfrac{\mu_0}{2} I_5 & \text{if} \quad J = 1 \\ +\infty & \text{otherwise} \end{cases}, \tag{40}$$

where $I_1 = \mathbf{F}\cdot\mathbf{F}$, $I_5 = \mathbf{F}^{-T}\mathbf{H}\cdot\mathbf{F}^{-T}\mathbf{H}$, $J = \det\mathbf{F}$ and where G and $\mu_0 = 4\pi\times 10^{-7}$ H/m stand for the initial shear modulus of the rubber and the permeability of vacuum, respectively. On the other hand, we model the ferrofluid inclusions with the Langevin-type free-energy function

$$W_\mathrm{i}(\mathbf{F},\mathbf{0},\mathbf{H}) = \begin{cases} -\mathcal{S}(I_5) = -\dfrac{\mu_0}{2} I_5 - \dfrac{\mu_0^2 m_s^2}{3(\mu_\mathrm{i}-\mu_0)} \ln\left[\dfrac{\sinh\left[3(\mu_\mathrm{i}-\mu_0)\sqrt{I_5}/(\mu_0 m_s)\right]}{3(\mu_\mathrm{i}-\mu_0)\sqrt{I_5}/(\mu_0 m_s)}\right] & \text{if} \quad J = 1 \\ +\infty & \text{otherwise} \end{cases}, \tag{41}$$

where μ_i denotes the initial magnetic permeability of the inclusions, while m_s stands for the saturated value of their magnetization $\mathbf{m}_\mathrm{i} = [2\mathcal{S}'(I_5)/\mu_0 - 1]\mathbf{F}^{-T}\mathbf{H}$ at large magnetic fields. Given that the spatial distribution of inclusions is isotropic, we also have that

$$\nu(\boldsymbol{\xi}) = \frac{1}{4\pi}.$$

Upon substituting the above constitutive and microstructural inputs in the general HJ equation (1)–(2), it is not difficult to deduce that its viscosity solution $W = +\infty$ for deformations with $J \neq 1$, while for isochoric deformations when $J = 1$, with a slight abuse of notation, it can be written rather compactly in the form

$$W(\mathbf{F},\mathbf{0},\mathbf{H},c) = 2G\,V(\lambda_1,\lambda_2,H_1,H_2,H_3,c) + \frac{G}{2}\left[\lambda_1^2+\lambda_2^2+\frac{1}{\lambda_1^2\lambda_2^2}-3\right] - \frac{\mu_0}{2}\left[\frac{H_1^2}{\lambda_1^2}+\frac{H_2^2}{\lambda_2^2}+\lambda_1^2\lambda_2^2 H_3^2\right]. \tag{42}$$

Table 1
Material parameters and volume fraction of ferrofluid inclusions.

G (kPa)	μ_i/μ_0	m_s (MA/m)	c
0.025	10	0.3	0.15

Here, λ_1 and λ_2 stand for two of the singular values of the deformation gradient tensor $\mathbf{F}$ (in view of the condition that $J = 1$, the third singular value is such that $\lambda_3 = 1/(\lambda_1\lambda_2)$), H_1, H_2, H_3 denote the three components of the Lagrangian magnetic field $\mathbf{H}$ with respect to the Lagrangian principal axes (that is, the principal axes of $\mathbf{F}^T\mathbf{F}$), while $V = V(\lambda_1, \lambda_2, H_1, H_2, H_3, \mathtt{c})$ stands for the viscosity solution of the following HJ equation:

$$\begin{cases} \dfrac{\partial V}{\partial \mathtt{c}} + \mathcal{H}\left(\lambda_1, \lambda_2, H_1, H_2, H_3, \mathtt{c}, V, \dfrac{\partial V}{\partial \lambda_1}, \dfrac{\partial V}{\partial \lambda_2}, \dfrac{\partial V}{\partial H_1}, \dfrac{\partial V}{\partial H_2}, \dfrac{\partial V}{\partial H_3}\right) = 0, \\ \quad \{\lambda_1, \lambda_2, H_1, H_2, H_3\} \in \mathfrak{S}, \quad \mathtt{c} \in \mathfrak{T} \\ V(\lambda_1, \lambda_2, H_1, H_2, H_3, 1) = -\dfrac{1}{4}\left[\lambda_1^2 + \lambda_2^2 + \dfrac{1}{\lambda_1^2\lambda_2^2} - 3\right] + \dfrac{\mu_0}{4G}\left[\dfrac{H_1^2}{\lambda_1^2} + \dfrac{H_2^2}{\lambda_2^2} + \lambda_1^2\lambda_2^2 H_3^2\right] - \\ \qquad\qquad \dfrac{1}{2G}\mathcal{S}\left(\dfrac{H_1^2}{\lambda_1^2} + \dfrac{H_2^2}{\lambda_2^2} + \lambda_1^2\lambda_2^2 H_3^2\right) \\ \quad \{\lambda_1, \lambda_2, H_1, H_2, H_3\} \in \mathfrak{S} \end{cases}, \tag{43}$$

where $\mathfrak{S} = \{\lambda_1 \in \mathbb{R}^+, \lambda_2 \in \mathbb{R}^+, H_1 \in \mathbb{R}, H_2 \in \mathbb{R}, H_3 \in \mathbb{R}\}$ and $\mathfrak{T} = [c, 1)$, with Hamiltonian

$$\mathcal{H} = -\frac{1}{\mathtt{c}}V - \sum_{\substack{m,n,p,q,r=0 \\ m+n+p+q+r=2}}^{2} \frac{\beta_{mnpqr}}{\mathtt{c}}\left(\frac{\partial V}{\partial \lambda_1}\right)^m\left(\frac{\partial V}{\partial \lambda_2}\right)^n\left(\frac{\partial V}{\partial H_1}\right)^p\left(\frac{\partial V}{\partial H_2}\right)^q\left(\frac{\partial V}{\partial H_3}\right)^r; \tag{44}$$

due to their bulkiness, the expressions for the fifteen coefficients $\beta_{mnpqr} = \beta_{mnpqr}(\lambda_1, \lambda_2, H_1, H_2, H_3)$ entering in the Hamiltonian (44) are spelled out in Appendix C.

Thus, the computation of the homogenized free-energy function (42) characterizing the macroscopic magneto-elastic response of the above-described magnetorheological elastomer filled with ferrofluid inclusions amounts to solving the HJ equation (43)–(44) for the function V. Here, we do so by means of the proposed WENO scheme. To this end, we first make the change of "space" and "time" variables

$$x = \ln\left(\frac{\lambda_1}{\lambda_2}\right), \quad y = \ln\left(\lambda_1\lambda_2^2\right), \quad \mathtt{t} = -\ln \mathtt{c}$$

in (43)–(44) so as to have symmetry for compressive ($\lambda_1, \lambda_2 < 1$) and tensile deformations ($\lambda_1, \lambda_2 > 1$) as well as to circumvent dealing with the factor $1/\mathtt{c}$ in (44). For possible comparison with experiments, we set the rubber and ferrofluid material parameters as well as the volume fraction of the inclusions to those listed in Table 1. Finally, we choose the following computational domains

$$\mathfrak{S}^h = \{(x_i, y_j, H_{1_p}, H_{2_q}, H_{3_r}) : x_i = ih,\ y_j = jh,\ H_{1_p} = ph\,\mathrm{MA/}m,\ H_{2_q} = qh\,\mathrm{MA/}m,\ H_{3_r} = rh\,\mathrm{MA/}m,$$

$$0 \le i, j, p, q, r \le M,\ Mh = 1.5\}$$

and

$$\mathfrak{T}^\delta = \{\mathtt{t}^k : \mathtt{t}^k = k\Delta\mathtt{t},\ 1 \le k \le T,\ T\Delta\mathtt{t} = 1.897\}$$

with $h = 0.05$ and $\Delta\mathtt{t} = h/2 = 0.025$. For illustration purposes, Fig. 6 shows the solution (42) generated by the WENO scheme for the case when $H_1 = H_2 = H_3 = 0$ MA/m in part (a) and the case when $\lambda_2 = \lambda_1^{-1/2}$ and $H_2 = H_3 = 0$ MA/m in part (b). As expected, the computed W exhibits a fairly high degree of regularity but exhibits as well steep gradients in its "space" variables. This warrants employing a WENO scheme such as the one proposed in this work.

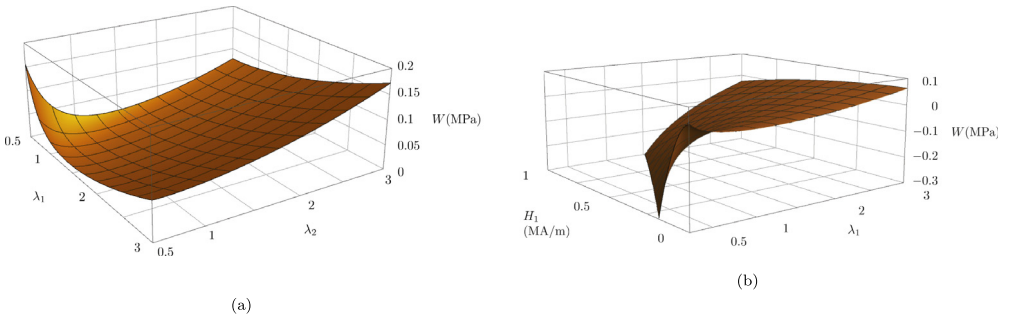

Fig. 6. WENO finite-difference solution of the homogenized free-energy function (42) describing the macroscopic magneto-elastic response of a Gaussian rubber, characterized by the free-energy function (40), filled with an isotropic distribution of ferrofluid inclusions, characterized by the free-energy function (41), with the material parameters and volume fraction of inclusions listed in Table 1. Part (a) shows W as a function of λ_1 and λ_2 for the case when $H_1 = H_2 = H_3 = 0$ MA/m, whereas part (b) shows W as a function of λ_1 and H_1 for the case when $\lambda_2 = \lambda_1^{-1/2}$ and $H_2 = H_3 = 0$ MA/m.

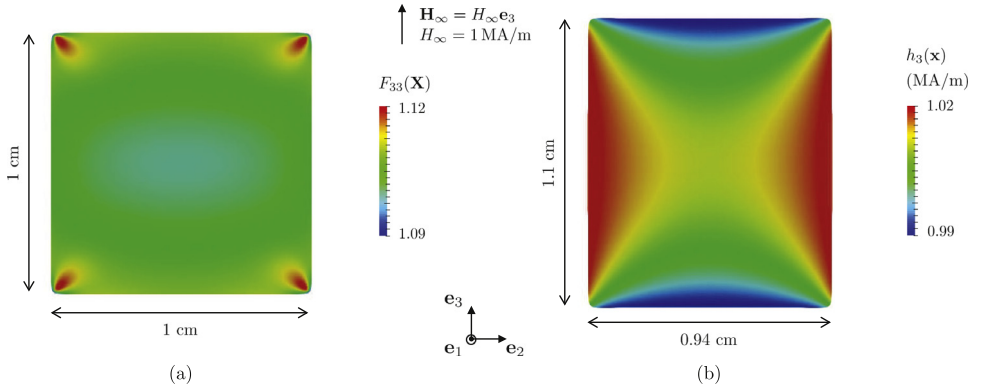

Fig. 7. Contour plots of the components $F_{33}(\mathbf{X})$ and $h_3(\mathbf{x})$ of the deformation gradient tensor and the Eulerian magnetic field in the $\mathbf{e}_2$–$\mathbf{e}_3$ plane, respectively, over: (a) the undeformed configuration and (b) the deformed configuration of the cylindrical specimen.

The FE computation of the macroscopic fields within the cylindrical specimen and surrounding air. Having worked out numerically the homogenized free energy W that describes the macroscopic magneto-elastic *material* response of the magnetorheological elastomer making up the cylindrical specimen, we are now in a position to investigate the magneto-elastic *structural* response of the specimen when subjected to a remotely applied uniaxial magnetic field, say $\mathbf{H}_\infty = H_\infty \mathbf{e}_3$. Again, because the deformation and magnetic fields inside the specimen, as well as in the surrounding air, are expected to be *non-uniform*, generating solutions for this boundary-value problem requires an additional numerical treatment. Here, we employ a FE formulation to discretize the relevant magneto-elastostatics equations and generate solutions for the deformation and magnetic fields at every material point in both the cylindrical specimen and the surrounding air; the interested reader is referred to Section 6 in [35] and Section 5 and Appendix in [58] for the relevant technical details on the FE formulation. For possible comparison with experiments, we consider the case of a cylindrical specimen with equal initial diameter and initial height of 1 cm (featuring filleted edges to avoid singularities) whose longitudinal axis is aligned in the direction of the applied magnetic field, here, $\mathbf{H}_\infty = H_\infty \mathbf{e}_3$ with $H_\infty = 1$ MA/m; see Fig. 5.

Fig. 7(a) shows contour plots of the component $F_{33}(\mathbf{X})$ of the deformation gradient in the $\mathbf{e}_2$–$\mathbf{e}_3$ plane over the *undeformed* configuration of the specimen. On the other hand, Fig. 7(b) shows contour plots of the component $h_3(\mathbf{x})$ of the Eulerian magnetic field $\mathbf{h} = \mathbf{F}^{-T}\mathbf{H}$ in the same $\mathbf{e}_2$–$\mathbf{e}_3$ plane but over the *deformed* configuration of the specimen. A first immediate observation from Fig. 7 is that the specimen undergoes a substantial elongation in the direction of the applied magnetic field, even though its intensity $H_\infty = 1$ MA/m is moderate. It is also plain that while the deformation and the Eulerian magnetic fields are *not* uniform over the specimen, they fluctuate over

relatively narrow ranges of values. Both of these features are in direct contrast with the behavior of comparable cylindrical specimens made up of classical magnetorheological elastomers filled with iron particles (cf. Section 7 in [35]), and hence point to the further investigation of magnetorheological elastomers filled with ferrofluid inclusions. By the same token, the above sample results provide ample motivation to further make use of the proposed WENO scheme to generate numerical solutions for the general HJ equation (1)–(2) in order to investigate an admittedly wide range of nonlinear and coupled phenomena in solids; see, e.g., [59] for a recent application to porous elastomers in $N = 3$ dimensions.

Acknowledgments

Support for this work by the National Science Foundation, United States through the Grant CMMI–1661853 is gratefully acknowledged. V.L. would also like to acknowledge support from the Hibbitt Engineering Fellowship at Brown University, United States.

Appendix A. WENO approximation formulas for the "boundary" grid points

In this appendix, we report the fifth-order accurate left-biased and right-biased WENO approximations of the first derivative $u_x(x)$ of a single-variable scalar function $u(x)$ at the corresponding "boundary" grid points, other than at x_0, namely, at x_1, x_2, x_{M-1}, x_M for the left-biased WENO approximation and at x_1, x_{M-2}, x_{M-1}, x_M for the right-biased WENO approximation. As already mentioned in the main body of the text, the derivations of these approximations follow closely that of the WENO approximations worked out for $u_x(x_0)$ in Section 3.1 and hence we do not repeat them here. Instead, we report directly the resulting formulas.

The left-biased and right-biased WENO approximations of the first derivative of $u(x)$ at x_1 can be compactly written in the form

$$u^-_{x,1} = u^+_{x,1} = \frac{11}{6}\frac{\Delta^+ u_1}{h} - \frac{7}{6}\frac{\Delta^+ u_2}{h} + \frac{1}{3}\frac{\Delta^+ u_3}{h} - g_1\left(\frac{\Delta^-\Delta^+ u_1}{h}, \frac{\Delta^-\Delta^+ u_2}{h}, \frac{\Delta^-\Delta^+ u_3}{h}, \frac{\Delta^-\Delta^+ u_4}{h}\right),$$

where

$$g_1(z_1, z_2, z_3, z_4) = \frac{1}{3}\widehat{\omega}_{3,1}\,(z_1 - 2z_2 + z_3) - \frac{11}{6}\widehat{\omega}_{5,1}\,(z_2 - 2z_3 + z_4) \tag{45}$$

with the parameters

$$\widehat{\omega}_{j,1} = \frac{\dfrac{\gamma_{j,1}}{(\epsilon + h^2\widehat{\mathcal{S}}_{j,1})^2}}{\sum_{k=3}^{6}\dfrac{\gamma_{k,1}}{(\epsilon + h^2\widehat{\mathcal{S}}_{k,1})^2}}, \quad \gamma_{3,1} = \frac{3}{5}, \quad \gamma_{4,1} = \frac{47}{110}, \quad \gamma_{5,1} = -\frac{3}{110}, \tag{46}$$

and the smoothness indicators

$$\widehat{\mathcal{S}}_{j,1} = \frac{13}{12}\left(z_{j-2} - z_{j-1}\right)^2 + \left[(j-2)z_{j-2} - (j-3)z_{j-1}\right]^2, \tag{47}$$

where, again, the explicit dependence of $\widehat{\omega}_{j,1}$ and $\widehat{\mathcal{S}}_{j,1}$ on $z_1, \ldots, z_4$ has been omitted for notational convenience.

Similarly, the left-biased WENO approximation of $u_x(x_2)$ can be written as

$$u^-_{x,2} = -\frac{1}{12}\frac{\Delta^+ u_3}{h} + \frac{1}{7}\frac{\Delta^+ u_2}{h} + \frac{1}{7}\frac{\Delta^+ u_1}{h} - \frac{1}{12}\frac{\Delta^+ u_0}{h} + g\left(\frac{\Delta^-\Delta^+ u_4}{h}, \frac{\Delta^-\Delta^+ u_3}{h}, \frac{\Delta^-\Delta^+ u_2}{h}, \frac{\Delta^-\Delta^+ u_1}{h}\right)$$

and the right-biased WENO approximation of $u_x(x_{M-2})$ reads as

$$u^+_{x,M-2} = -\frac{1}{12}\frac{\Delta^+ u_{M-4}}{h} + \frac{7}{12}\frac{\Delta^+ u_{M-3}}{h} + \frac{7}{12}\frac{\Delta^+ u_{M-2}}{h} - \frac{1}{12}\frac{\Delta^+ u_{M-1}}{h} - g\left(\frac{\Delta^-\Delta^+ u_{M-4}}{h}, \frac{\Delta^-\Delta^+ u_{M-3}}{h}, \frac{\Delta^-\Delta^+ u_{M-2}}{h}, \frac{\Delta^-\Delta^+ u_{M-1}}{h}\right),$$

where we recall that the function g is given by expressions (13) with (10) and (14).

Finally, the left-biased and right-biased WENO approximations of $u_x(x_{M-1})$ and $u_x(x_M)$ are given by

$$u^-_{x,M-1} = u^+_{x,M-1} = \frac{11}{6}\frac{\Delta^+ u_{M-2}}{h} - \frac{7}{6}\frac{\Delta^+ u_{M-3}}{h} + \frac{1}{3}\frac{\Delta^+ u_{M-4}}{h} + g_1\left(\frac{\Delta^-\Delta^+ u_{M-1}}{h}, \frac{\Delta^-\Delta^+ u_{M-2}}{h}, \frac{\Delta^-\Delta^+ u_{M-3}}{h}, \frac{\Delta^-\Delta^+ u_{M-4}}{h}\right),$$

$$u^-_{x,M} = u^+_{x,M} = \frac{13}{3}\frac{\Delta^+ u_{M-2}}{h} - \frac{31}{6}\frac{\Delta^+ u_{M-3}}{h} + \frac{11}{6}\frac{\Delta^+ u_{M-4}}{h} + g_0\left(\frac{\Delta^-\Delta^+ u_{M-1}}{h}, \frac{\Delta^-\Delta^+ u_{M-2}}{h}, \frac{\Delta^-\Delta^+ u_{M-3}}{h}, \frac{\Delta^-\Delta^+ u_{M-4}}{h}\right),$$

where, again, the function g_1 is given by expressions (45) through (47) and where we recall that the function g_0 is given by expressions (20) with (18) and (21).

Appendix B. Identification and computation of "inflow" boundary conditions on $\partial\mathfrak{S}^h$ via the method of characteristics

As discussed in Section 3.4, for a given choice of "space" discretization $\mathfrak{S}^h$, the value of the function W needs to be prescribed on the regions of the boundary $\partial\mathfrak{S}^h$ through which the characteristics pass in the "inflow" direction so as to ensure the well-posedness of the numerical scheme. These boundary conditions need to be identified and computed *a priori* for all the discrete "times" in the given choice of discretized "time" domain $\mathfrak{T}^\delta$. In this appendix, we sketch out how to carry out such identifications and computations via the method of characteristics. For clarity of exposition, we present the relevant basic details for the case when the HJ equation (1)–(2) involves only two "space" variables, and use the HJ equation (36)–(37) examined in Section 4 as an illustrative example.

The basic idea behind the method of characteristics is to recast (appropriate types of) PDEs as a system of ordinary differential equations (ODEs); see, e.g., [60] for an interesting historical perspective on this method. For the type of HJ equation (1)–(2) under investigation here, the method amounts to finding curves in $\mathfrak{S}\times\mathfrak{T}$, the so-called characteristics, along which the solution W can be computed. This is achieved by integrating the system of ODEs – with unknowns, the "space" and "time" variables, the solution of the PDE, and its partial "space"-"time" first-order derivatives – defining these curves from a point $(x_0, y_0)\in\mathfrak{S}$ where the initial condition is prescribed, to points $(x, y, \mathtt{t})$ in $\mathfrak{S}\times\mathfrak{T}$. Repeating this process for different initial points $(x_0, y_0)\in\mathfrak{S}$ allows one to compute, in principle, the solution W in the whole of $\mathfrak{S}\times\mathfrak{T}$. We do not discuss further this classical method and, instead, refer the interested reader to Section 3.2 in [7] for the derivation of the results spelled-out below as well as for additional details regarding the existence and uniqueness aspects of the resulting solutions.

We begin by writing the HJ equation of interest here in the form

$$\begin{cases} \mathcal{F}(p, q, r, z, x, y, \mathtt{t}) = r + \mathcal{H}(x, y, z, p, q) = 0, \quad (x, y)\in\mathfrak{S}, \quad \mathtt{t}\in\mathfrak{T} \\ z_0 = W_{\mathtt{i}}(x_0, y_0), \quad \{x_0, y_0\}\in\mathfrak{S} \end{cases}$$

with the parametrization

$$p(s) = \frac{\partial W}{\partial x}(x(s), y(s), \mathtt{t}(s)), \quad q(s) = \frac{\partial W}{\partial y}(x(s), y(s), \mathtt{t}(s)),$$

$$r(s) = \frac{\partial W}{\partial \mathtt{t}}(x(s), y(s), \mathtt{t}(s)), \quad z(s) = W(x(s), y(s), \mathtt{t}(s)), \quad s\geq 0$$

along the characteristic curve $(x(s), y(s), \mathtt{t}(s))$; in these expressions, we have made use of the notation $z_0 = z(0)$, $x_0 = x(0)$, $y_0 = y(0)$, $\mathtt{t}_0 = \mathtt{t}(0)$. Now, the characteristic curve initiating from $(x_0, y_0)\in\mathfrak{S}$ is defined by the system

of ODEs

$$\begin{cases} \dfrac{\mathrm{d}p}{\mathrm{d}s} = -\dfrac{\partial \mathcal{F}}{\partial x} - p\dfrac{\partial \mathcal{F}}{\partial z} = -\dfrac{\partial \mathcal{H}}{\partial x} - p\dfrac{\partial \mathcal{H}}{\partial z} \\ \dfrac{\mathrm{d}q}{\mathrm{d}s} = -\dfrac{\partial \mathcal{F}}{\partial y} - q\dfrac{\partial \mathcal{F}}{\partial z} = -\dfrac{\partial \mathcal{H}}{\partial y} - q\dfrac{\partial \mathcal{H}}{\partial z} \\ \dfrac{\mathrm{d}r}{\mathrm{d}s} = -\dfrac{\partial \mathcal{F}}{\partial \mathtt{t}} - r\dfrac{\partial \mathcal{F}}{\partial z} = -r\dfrac{\partial \mathcal{H}}{\partial z} \\ \dfrac{\mathrm{d}z}{\mathrm{d}s} = p\dfrac{\partial \mathcal{F}}{\partial p} + q\dfrac{\partial \mathcal{F}}{\partial q} + r\dfrac{\partial \mathcal{F}}{\partial r} = p\dfrac{\partial \mathcal{H}}{\partial p} + q\dfrac{\partial \mathcal{H}}{\partial q} + r \\ \dfrac{\mathrm{d}x}{\mathrm{d}s} = \dfrac{\partial \mathcal{F}}{\partial p} = \dfrac{\partial \mathcal{H}}{\partial p} \\ \dfrac{\mathrm{d}y}{\mathrm{d}s} = \dfrac{\partial \mathcal{F}}{\partial q} = \dfrac{\partial \mathcal{H}}{\partial q} \\ \dfrac{\mathrm{d}\mathtt{t}}{\mathrm{d}s} = \dfrac{\partial \mathcal{F}}{\partial \mathtt{t}} = 1 \end{cases} \tag{48}$$

together with the compatibility equations

$$\mathcal{F}(p_0, q_0, r_0, z_0, x_0, y_0, \mathtt{t}_0) = r_0 + \mathcal{H}(x_0, y_0, z_0, p_0, q_0) = 0,$$

$$p_0 = \frac{\partial W_{\mathtt{i}}}{\partial x}(x_0, y_0, \mathtt{t}_0), \quad q_0 = \frac{\partial W_{\mathtt{i}}}{\partial y}(x_0, y_0, \mathtt{t}_0) \tag{49}$$

that define $p_0 = p(0)$, $q_0 = q(0)$, $r_0 = r(0)$. With help of the above formulation, the "inflow" regions of the boundary $\partial\mathfrak{S}^h$ of the computational domain $\mathfrak{S}^h$ where boundary conditions need to be prescribed can then be readily identified as those that satisfy the condition

$$\begin{pmatrix} \dfrac{\mathrm{d}x}{\mathrm{d}s}(s) \\ \dfrac{\mathrm{d}y}{\mathrm{d}s}(s) \end{pmatrix} \cdot \mathbf{n}^h < 0, \tag{50}$$

where $\mathbf{n}^h$ denotes the outward unit normal to $\partial\mathfrak{S}^h$.

The "inflow" boundary conditions for the HJ equation (36)–(37). By way of an example, we spell out the specialization of the general system of characteristics (48)–(49) to the case of the HJ equation (36)–(37) studied in Section 4:

$$\begin{cases} \dfrac{\mathrm{d}p}{\mathrm{d}s} = \dfrac{G}{2}e^{y}\sinh x + \left(\dfrac{e^{-y}}{2\cosh^2(x/2)} - 1\right)p + \dfrac{e^{-y}\tanh(x/2)}{4G\cosh^2(x/2)}p^2 \\ \dfrac{\mathrm{d}q}{\mathrm{d}s} = \dfrac{G}{2}\left[e^{y}\cosh(x) - e^{-y}\right] - e^{-y}\tanh\left(\dfrac{x}{2}\right)p + \dfrac{e^{-y}}{4G\cosh^2(x/2)}p^2 + (e^{-y} - 1)q \\ \dfrac{\mathrm{d}r}{\mathrm{d}s} = -r \\ \dfrac{\mathrm{d}z}{\mathrm{d}s} = -e^{-y}\tanh\left(\dfrac{x}{2}\right)p + \dfrac{e^{-y}}{2G\cosh^2(x/2)}p^2 + (e^{-y} - 1)q + r \\ \dfrac{\mathrm{d}x}{\mathrm{d}s} = -e^{-y}\tanh\left(\dfrac{x}{2}\right) + \dfrac{e^{-y}}{2G\cosh^2(x/2)}p \\ \dfrac{\mathrm{d}y}{\mathrm{d}s} = e^{-y} - 1 \\ \dfrac{\mathrm{d}\mathtt{t}}{\mathrm{d}s} = \dfrac{\partial \mathcal{F}}{\partial \mathtt{t}} = 1 \end{cases} \tag{51}$$

with

$$p_0 = 0,\ q_0 = 0,\ r_0 = \frac{G}{2}\left[e^{y_0}\cosh x_0 + e^{-y_0} - 2\right],\ z_0 = 0,\ \mathtt{t}_0 = 0.$$

Although it is possible from knowledge of the solution (38) for W to work out a closed-form solution for the system of nonlinear ODEs (51), it is also straightforward – and in general required – to integrate numerically this system to identify and compute the required "inflow" boundary conditions. Now, for the choice of discretized "space" domain (39) considered in Section 4.2, it follows from the condition (50) that boundary conditions need *not* be prescribed at the boundary grid points $(x_i, y_j) = (0, y_j)$ and $(x_i, y_j) = (x_i, 0)$ for any "time" $\mathfrak{t}^k$. On the other hand, the value of W needs to be prescribed on "time"-dependent parts of the boundary grid points $(x_i, y_j) = (2, y_j)$, while it needs to be prescribed for all "times" $\mathfrak{t}^k \in \mathfrak{T}^\delta$ at the boundary grid points $(x_i, y_j) = (x_i, 2)$.

We close by remarking that employing the above-outlined method of characteristics to compute the solution W in the entire computational domain of interest $\mathfrak{S}^h \times \mathfrak{T}^\delta$, and not just at the "inflow" boundaries on $\partial\mathfrak{S}^h$, is plausible but impractical, among other things, because it is computationally very costly, especially for problems with a large number of "space" variables.

Appendix C. The fifteen coefficients β_{mnpqr} in the Hamiltonian (44)

$$\beta_{20000} = \frac{2\Gamma_E\lambda_1^3\lambda_2\left(\lambda_1^4\lambda_2^8 - 2\lambda_1^6\lambda_2^6 + 2\lambda_1^4\lambda_2^2 - 1\right)}{3\left(\lambda_1^2-\lambda_2^2\right)^2\left(\lambda_1^4\lambda_2^2-1\right)^2} - \frac{\Gamma_F\lambda_1^5\lambda_2^3\left(3\lambda_1^4\lambda_2^2 - 2\lambda_1^2\lambda_2^4 - 1\right)}{3\left(\lambda_1^2-\lambda_2^2\right)\left(\lambda_1^4\lambda_2^2-1\right)^2} - \frac{\lambda_1^4\lambda_2^6 - 2\lambda_1^6\lambda_2^4 + \lambda_1^2\lambda_2^2 - \lambda_1^8\lambda_2^2 + \lambda_1^4}{3\left(\lambda_1^2-\lambda_2^2\right)^2\left(\lambda_1^4\lambda_2^2-1\right)},$$

$$\beta_{02000} = \frac{2\Gamma_E\lambda_1\lambda_2^3\left(\lambda_1^4\lambda_2^2 - 2\lambda_1^2\lambda_2^4 + 1\right)}{3\left(\lambda_1^2-\lambda_2^2\right)^2\left(\lambda_1^2\lambda_2^4-1\right)} - \frac{\Gamma_F\lambda_1^3\lambda_2^5}{3\left(\lambda_1^2-\lambda_2^2\right)\left(\lambda_1^2\lambda_2^4-1\right)} - \frac{\lambda_1^6\lambda_2^4 - 2\lambda_1^4\lambda_2^6 + \lambda_1^2\lambda_2^2 - \lambda_1^2\lambda_2^8 + \lambda_2^4}{3\left(\lambda_1^2-\lambda_2^2\right)^2\left(\lambda_1^2\lambda_2^4-1\right)},$$

$$\beta_{11000} = \frac{2\Gamma_E\lambda_1^2\lambda_2^2\left(\lambda_1^4\lambda_2^2 + \lambda_1^2\lambda_2^4 - 2\right)}{3\left(\lambda_1^2-\lambda_2^2\right)^2\left(\lambda_1^4\lambda_2^2-1\right)} + \frac{2\Gamma_F\lambda_1^4\lambda_2^4}{3\left(\lambda_1^2-\lambda_2^2\right)\left(\lambda_1^4\lambda_2^2-1\right)} - \frac{2\lambda_1\lambda_2\left(\lambda_1^2+\lambda_2^2\right)}{3\left(\lambda_1^2-\lambda_2^2\right)^2},$$

$$\beta_{00200} = \frac{\Gamma_E\lambda_1^3\lambda_2\left(\lambda_1^2\lambda_2^4-1\right)}{\left(\lambda_1^2-\lambda_2^2\right)\left(\lambda_1^4\lambda_2^2-1\right)}\left[\frac{2H_1^2\left(\lambda_1^4\lambda_2^8 - 2\lambda_1^6\lambda_2^6 + 2\lambda_1^4\lambda_2^2 - 1\right)}{3\lambda_1^2\left(\lambda_1^2-\lambda_2^2\right)\left(\lambda_1^4\lambda_2^2-1\right)\left(\lambda_1^2\lambda_2^4-1\right)} + \frac{H_2^2\left(\lambda_1^2+\lambda_2^2\right)^2\left(\lambda_1^4\lambda_2^2+\lambda_1^2\lambda_2^4-2\right)}{3\lambda_2^2\left(\lambda_1^2-\lambda_2^2\right)^3\left(\lambda_1^2\lambda_2^4-1\right)} - \frac{H_3^2\lambda_1^4\lambda_2^4\left(\lambda_1^4\lambda_2^2+1\right)^2\left(\lambda_1^4\lambda_2^2 - 2\lambda_1^2\lambda_2^4 + 1\right)}{3\left(\lambda_1^4\lambda_2^2-1\right)^3\left(\lambda_1^2\lambda_2^4-1\right)} - \frac{G}{\mu_0}\right] + \frac{\Gamma_F\lambda_1^5\lambda_2^3}{\lambda_1^4\lambda_2^2-1}\left[\frac{H_1^2\left(2\lambda_1^2\lambda_2^4 - 3\lambda_1^4\lambda_2^2 + 1\right)}{3\lambda_1^2\left(\lambda_1^4\lambda_2^2-1\right)\left(\lambda_1^2-\lambda_2^2\right)} + \frac{H_2^2\left(\lambda_1^2+\lambda_2^2\right)^2}{3\lambda_2^2\left(\lambda_1^2-\lambda_2^2\right)^3} + \frac{2H_3^2\lambda_1^4\lambda_2^4\left(\lambda_1^4\lambda_2^2+1\right)^2}{3\left(\lambda_1^4\lambda_2^2-1\right)^3} - \frac{G}{\mu_0}\right] + \frac{\lambda_1^2\lambda_2^2}{\lambda_1^2-\lambda_2^2}\left[\frac{H_1^2\left(\lambda_1^6\lambda_2^2 + 2\lambda_1^4\lambda_2^4 - \lambda_1^2\lambda_2^6 - \lambda_1^2 - \lambda_2^2\right)}{3\lambda_1^2\lambda_2^2\left(\lambda_1^2-\lambda_2^2\right)\left(\lambda_1^4\lambda_2^2-1\right)} - \frac{4H_2^2\lambda_1^2\left(\lambda_1^2+\lambda_2^2\right)}{3\lambda_2^2\left(\lambda_1^2-\lambda_2^2\right)^3} + \frac{H_3^2\lambda_1^{10}\lambda_2^2\left(\lambda_1^8\lambda_2^4 - 2\lambda_1^6\lambda_2^6 - 2\lambda_1^2\lambda_2^4 - 1\right)}{3\lambda_1^4\left(\lambda_1^4\lambda_2^2-1\right)^3} + \frac{G}{\mu_0}\right],$$

$$\beta_{00020} = \frac{\Gamma_E\lambda_1\lambda_2^3}{\lambda_1^2-\lambda_2^2}\left[\frac{H_1^2\left(\lambda_1^2+\lambda_2^2\right)^2\left(\lambda_1^4\lambda_2^2+\lambda_1^2\lambda_2^4-2\right)}{3\lambda_1^2\left(\lambda_1^2-\lambda_2^2\right)^3\left(\lambda_1^4\lambda_2^2-1\right)} + \frac{H_3^2\lambda_1^4\lambda_2^4\left(\lambda_1^2\lambda_2^4 - 2\lambda_1^4\lambda_2^2 + 1\right)\left(\lambda_1^2\lambda_2^4+1\right)^2}{3\left(\lambda_1^4\lambda_2^2-1\right)\left(\lambda_1^2\lambda_2^4-1\right)^3} + \frac{2H_2^2\left(\lambda_1^4\lambda_2^2 - 2\lambda_1^2\lambda_2^4 + 1\right)}{3\lambda_2^2\left(\lambda_1^2\lambda_2^4-1\right)\left(\lambda_1^2-\lambda_2^2\right)} + \frac{G}{\mu_0}\right] + \frac{\Gamma_F\lambda_1^3\lambda_2^3}{3\left(\lambda_1^2\lambda_2^4-1\right)}\left[\frac{H_1^2\lambda_2^2\left(\lambda_1^2+\lambda_2^2\right)^2\left(\lambda_1^2\lambda_2^4-1\right)}{\lambda_1^2\left(\lambda_1^2-\lambda_2^2\right)^3\left(\lambda_1^4\lambda_2^2-1\right)} - \frac{H_2^2}{\lambda_1^2-\lambda_2^2} +$$

$$\frac{H_3^2\lambda_1^4\lambda_2^6\left(\lambda_1^2\lambda_2^4+1\right)^2}{\left(\lambda_1^2\lambda_2^4-1\right)^2\left(\lambda_1^4\lambda_2^2-1\right)}\Bigg]-\frac{\lambda_1^2\lambda_2^2}{\lambda_1^2-\lambda_2^2}\Bigg[\frac{4H_1^2\lambda_2^2\left(\lambda_1^2+\lambda_2^2\right)}{3\lambda_1^2\left(\lambda_1^2-\lambda_2^2\right)^3}+\frac{H_2^2\left(\lambda_1^6\lambda_2^2-2\lambda_1^4\lambda_2^4-\lambda_1^2\lambda_2^6+\lambda_1^2+\lambda_2^2\right)}{3\lambda_1^2\lambda_2^2\left(\lambda_1^2-\lambda_2^2\right)\left(\lambda_1^2\lambda_2^4-1\right)}-$$

$$\frac{H_3^2\lambda_1^2\lambda_2^6\left(2\lambda_1^6\lambda_2^6-\lambda_1^4\lambda_2^8+2\lambda_1^4\lambda_2^2+1\right)}{3\left(\lambda_1^2\lambda_2^4-1\right)^3}+\frac{G}{\mu_0}\Bigg],$$

$$\beta_{00002}=-\frac{\Gamma_E\lambda_1\lambda_2}{\lambda_1^4\lambda_2^2-1}\Bigg[\frac{H_1^2\left(\lambda_1^4\lambda_2^2+1\right)^2\left(\lambda_1^4\lambda_2^2-2\lambda_1^2\lambda_2^4+1\right)}{3\lambda_1^2\left(\lambda_1^2-\lambda_2^2\right)\left(\lambda_1^4\lambda_2^2-1\right)^3}+\frac{H_2^2\left(\lambda_1^2\lambda_2^4+1\right)^2\left(2\lambda_1^4\lambda_2^2-\lambda_1^2\lambda_2^4-1\right)}{3\lambda_2^2\left(\lambda_1^2-\lambda_2^2\right)\left(\lambda_1^2\lambda_2^4-1\right)^3}-$$

$$\frac{2H_3^2\lambda_1^4\lambda_2^4\left(\lambda_1^4\lambda_2^2+\lambda_1^2\lambda_2^4-2\right)}{3\left(\lambda_1^4\lambda_2^2-1\right)\left(\lambda_1^2\lambda_2^4-1\right)}+\frac{G}{\mu_0}\Bigg]+\frac{\Gamma_F\lambda_1\lambda_2}{\lambda_1^4\lambda_2^2-1}\Bigg[\frac{2H_1^2\lambda_2^2\left(\lambda_1^4\lambda_2^2+1\right)^2}{3\left(\lambda_1^4\lambda_2^2-1\right)^3}+\frac{H_2^2\lambda_1^2\left(\lambda_1^2\lambda_2^4+1\right)^2}{3\left(\lambda_1^2\lambda_2^4-1\right)^3}-$$

$$\frac{H_3^2\lambda_1^4\lambda_2^4\left(\lambda_1^4\lambda_2^2+2\lambda_1^2\lambda_2^4-3\right)}{3\left(\lambda_1^4\lambda_2^2-1\right)\left(\lambda_1^2\lambda_2^4-1\right)}+\frac{G}{\mu_0}\Bigg]+\frac{H_1^2\left(\lambda_1^8\lambda_2^4-2\lambda_1^6\lambda_2^6-2\lambda_1^2\lambda_2^4-1\right)}{3\left(\lambda_1^2-\lambda_2^2\right)\left(\lambda_1^4\lambda_2^2-1\right)^3}+$$

$$\frac{H_2^2\left(2\lambda_1^6\lambda_2^6-\lambda_1^4\lambda_2^8+2\lambda_1^4\lambda_2^2+1\right)}{3\left(\lambda_1^2-\lambda_2^2\right)\left(\lambda_1^2\lambda_2^4-1\right)^3}-\frac{H_3^2\lambda_1^2\lambda_2^2\left(\lambda_1^6\lambda_2^2-\lambda_1^2\lambda_2^6-\lambda_1^2+\lambda_2^2\right)}{3\left(\lambda_1^2-\lambda_2^2\right)\left(\lambda_1^4\lambda_2^2-1\right)\left(\lambda_1^2\lambda_2^4-1\right)},$$

$$\beta_{00110}=-\frac{8H_1H_2}{3\left(\lambda_1^2-\lambda_2^2\right)^3}\Bigg[\frac{\Gamma_E\lambda_1^3\lambda_2^3\left(\lambda_1^4\lambda_2^2+\lambda_1^2\lambda_2^4-2\right)}{\left(\lambda_1^2-\lambda_2^2\right)\left(\lambda_1^4\lambda_2^2-1\right)}+\frac{\Gamma_F\lambda_1^5\lambda_2^5}{\lambda_1^4\lambda_2^2-1}+\frac{\left(\lambda_1^2+\lambda_2^2\right)\left(\lambda_1^4-6\lambda_1^2\lambda_2^2+\lambda_2^4\right)}{4\left(\lambda_1^2-\lambda_2^2\right)}\Bigg],$$

$$\beta_{00011}=\frac{8H_2H_3\lambda_1^2\lambda_2^2}{3\left(\lambda_1^2\lambda_2^4-1\right)^3}\Bigg[\frac{\Gamma_E\lambda_1^3\lambda_2^5\left(2\lambda_1^4\lambda_2^2-\lambda_1^2\lambda_2^4-1\right)}{\left(\lambda_1^2-\lambda_2^2\right)\left(\lambda_1^4\lambda_2^2-1\right)}-\frac{\Gamma_F\lambda_1^5\lambda_2^7}{\lambda_1^4\lambda_2^2-1}-\frac{\lambda_1^6\lambda_2^8-\lambda_1^4\lambda_2^{10}+4\lambda_1^4\lambda_2^4-\lambda_1^2+\lambda_2^2}{4\left(\lambda_1^2-\lambda_2^2\right)}\Bigg],$$

$$\beta_{00101}=\frac{8H_1H_3\lambda_1^2\lambda_2^2}{3\left(\lambda_1^4\lambda_2^2-1\right)^3}\Bigg[\frac{\Gamma_E\lambda_1^5\lambda_2^3\left(\lambda_1^4\lambda_2^2-2\lambda_1^2\lambda_2^4+1\right)}{\left(\lambda_1^2-\lambda_2^2\right)\left(\lambda_1^4\lambda_2^2-1\right)}-\frac{2\Gamma_F\lambda_1^7\lambda_2^5}{\lambda_1^4\lambda_2^2-1}-\frac{\lambda_1^{10}\lambda_2^4-\lambda_1^8\lambda_2^6-4\lambda_1^4\lambda_2^4-\lambda_1^2+\lambda_2^2}{4\left(\lambda_1^2-\lambda_2^2\right)}\Bigg],$$

$$\beta_{10100}=\frac{2H_1}{\lambda_1}\beta_{20000},\quad \beta_{10010}=\frac{H_2}{\lambda_2}\beta_{11000},\quad \beta_{10001}=-\frac{2H_3}{\lambda_1}\beta_{20000}-\frac{H_3}{\lambda_2}\beta_{11000},$$

$$\beta_{01100}=\frac{H_1}{\lambda_1}\beta_{11000},\quad \beta_{01010}=\frac{2H_2}{\lambda_2}\beta_{02000},\quad \beta_{01001}=-\frac{2H_3}{\lambda_2}\beta_{02000}-\frac{H_3}{\lambda_1}\beta_{11000}.$$

In the above expressions,

$$\Gamma_F=\frac{1}{\sqrt{1-\lambda_1^2\lambda_2^4}}\mathcal{E}_F\left\{\frac{\sqrt{\lambda_1^2\lambda_2^4-1}}{2\sqrt{1-\lambda_1^2\lambda_2^4}}\ln\left[2\lambda_1\lambda_2^2\left(\sqrt{\lambda_1^2\lambda_2^4-1}+\lambda_1\lambda_2^2\right)-1\right];\frac{\lambda_1^4\lambda_2^2-1}{\lambda_1^2\lambda_2^4-1}\right\},$$

$$\Gamma_E=\frac{1}{\sqrt{1-\lambda_1^2\lambda_2^4}}\mathcal{E}_E\left\{\frac{\sqrt{\lambda_1^2\lambda_2^4-1}}{2\sqrt{1-\lambda_1^2\lambda_2^4}}\ln\left[2\lambda_1\lambda_2^2\left(\sqrt{\lambda_1^2\lambda_2^4-1}+\lambda_1\lambda_2^2\right)-1\right];\frac{\lambda_1^4\lambda_2^2-1}{\lambda_1^2\lambda_2^4-1}\right\},$$

where the functions $\mathcal{E}_F$ and $\mathcal{E}_E$, stand for, respectively, the incomplete elliptic integrals of first and second kind:

$$\mathcal{E}_F\{\phi;\eta\}=\int_0^\phi[1-\eta^2\sin^2\theta]^{-1/2}\,\mathrm{d}\theta,\quad \mathcal{E}_E\{\phi;\eta\}=\int_0^\phi[1-\eta^2\sin^2\theta]^{1/2}\,\mathrm{d}\theta.$$

References

[1] O. Lopez-Pamies, Elastic dielectric composites: Theory and application to particle-filled ideal dielectrics, J. Mech. Phys. Solids 64 (2014) 61–82.
[2] M. Crandall, P. Lions, Viscosity solutions of HJ equations, Trans. Amer. Math. Soc. 277 (1983) 1–42.
[3] M. Bardi, I. Capuzzo-Dolcetta, Optimal Control and Viscosity Solutions of HJ-Bellman Equations, Springer, New York, 1997.
[4] S. Osher, R. Fedkiw, Level Set Methods and Dynamic Implicit Surfaces, Springer, New York, 2003.
[5] E.F. Toro, Riemann Solvers and Numerical Methods for Fluid Dynamics, Springer, New York, 2009.
[6] S.H. Benton, The HJ Equation: A Global Approach, Academic Press, New York, 1977.
[7] L.C. Evans, Partial Differential Equations, The American Mathematical Society, 2010.
[8] M. Crandall, P. Lions, Two approximations of solutions of HJ equations, Math. Comput. 43 (1984) 1–19.
[9] S. Osher, J. Sethian, Fronts propagating with curvature dependent speed: algorithms based on HJ formulations, J. Comput. Phys. 79 (1988) 12–49.
[10] G.-S. Jiang, D. Peng, Weighted ENO schemes for HJ equations, SIAM J. Sci. Comput. 21 (2000) 2126–2143.
[11] S. Bryson, D. Levy, High-order semi-discrete central-upwind schemes for multi-dimensional HJ equations, J. Comput. Phys. 189 (2003) 63–87.
[12] C. Hu, C.-W. Shu, A discontinuous Galerkin finite element method for Hamilton–Jacobi equations, SIAM J. Sci. Comput. 21 (1999) 666–690.
[13] M. Born, E. Wolf, A.B. Bhatia, Principles of Optics: Electromagnetic Theory of Propagation, Interference, and Diffraction of Light, Cambridge University Press, 2003.
[14] V.P. Maslov, M.V. Fedoriuk, Semi-Classical Approximation in Quantum Mechanics, Reidel, Dordrecht, 1981.
[15] W.H. Fleming, R. Rishel, Deterministic and Stochastic Optimal Control, Springer-Verlag, New York, 1975.
[16] D.A.G. Bruggeman, Berechnung verschiedener physikalischer Konstanten von heterogenen Substanzen. I. Dielektrizitätskonstanten und Leitfähigkeiten der Mischkörper aus isotropen Substanzen. [Calculation of various physical constants in heterogeneous substances. I. Dielectric constants and conductivity of composites from isotropic substances], Ann. Phys. 416 (1935) 636–664.
[17] A.N. Norris, A differential scheme for the effective moduli of composites, Mech. Mater. 4 (1985) 1–16.
[18] O. Lopez-Pamies, An exact result for the macroscopic response of particle-reinforced Neo-Hookean solids, J. Appl. Mech. 77 (2010) 021016.
[19] L. Tartar, in: P. Krée (Ed.), Estimations fines des coefficients homogénéisés, in: Ennio de Giorgi Colloquium, Research Notes in Mathematics, vol. 125, Pitman Publishing Ltd, London, 1985, pp. 168–187, [Fine estimations of homogenized coefficients].
[20] G.A. Francfort, F. Murat, Homogenization and optimal bounds in linear elasticity, Arch. Ration. Mech. Anal. 94 (1986) 307–334.
[21] G. deBotton, Transversely isotropic sequentially laminated composites in finite elasticity, J. Mech. Phys. Solids 53 (2005) 1334–1361.
[22] M.I. Idiart, Modeling the macroscopic behavior of two-phase nonlinear composites by infinite-rank laminates, J. Mech. Phys. Solids 56 (2008) 2599–2617.
[23] O. Lopez-Pamies, M.I. Idiart, An exact result for the macroscopic behavior of porous Neo-Hookean solids, J. Elast. 95 (2009) 99–105.
[24] O. Lopez-Pamies, M.I. Idiart, Fiber-reinforced hyperelastic solids: A realizable homogenization constitutive theory, Journal of Engineering Mathematics 68 (2010) 57–83.
[25] O. Lopez-Pamies, M.I. Idiart, T. Nakamura, Cavitation in elastomeric solids: I — A defect-growth theory, J. Mech. Phys. Solids 59 (2011a) 1464–1487.
[26] A. Dorfmann, R.W. Ogden, Nonlinear magnetoelastic deformations, Q. J. Mech. Appl. Math. 57 (2004) 599–622.
[27] A. Dorfmann, R.W. Ogden, Nonlinear electroelasticity, Acta Mech. 174 (2005) 167–183.
[28] O. Lopez-Pamies, Onset of cavitation in compressible, isotropic, hyperelastic solids, J. Elasticity 94 (2009) 115–145.
[29] O. Lopez-Pamies, T. Nakamura, M.I. Idiart, Cavitation in elastomeric solids: II — Onset-of-cavitation surfaces for Neo-Hookean materials, J. Mech. Phys. Solids 59 (2011b) 1488–1505.
[30] O. Lopez-Pamies, T. Goudarzi, T. Nakamura, The nonlinear elastic response of suspensions of rigid inclusions in rubber: I — An exact result for dilute suspensions, J. Mech. Phys. Solids 61 (2013) 1–18.
[31] S.A. Spinelli, O. Lopez-Pamies, A general closed-form solution for the overall response of piezoelectric composites with periodic and random particulate microstructures, Int. J. Solids Struct. 51 (2014) 2979–2989.
[32] S.A. Spinelli, V. Lefèvre, O. Lopez-Pamies, Dielectric elastomer composites: A general closed-form solution in the small-deformation limit, J. Mech. Phys. Solids 83 (2015) 263–284.
[33] V. Lefèvre, O. Lopez-Pamies, Nonlinear electroelastic deformations of dielectric elastomer composites: I — Ideal elastic dielectrics, J. Mech. Phys. Solids 99 (2017a) 409–437.
[34] J.S. Stratton, Electromagnetic Theory, McGraw-Hill, 1941.
[35] V. Lefèvre, K. Danas, O. Lopez-Pamies, A general result for the magnetoelastic response of isotropic suspensions of iron and ferrofluid particles in rubber, with applications to spherical and cylindrical specimens, J. Mech. Phys. Solids 107 (2017) 343–364.
[36] G.-S. Jiang, C.-W. Shu, Efficient implementation of weighted ENO schemes, J. Comput. Phys. 126 (1996) 202–228.
[37] X.-D. Liu, S. Osher, T. Chan, Weighted essentially non-oscillatory schemes, J. Comput. Phys. 115 (1994) 200–212.
[38] C.-W. Shu, High order weighted essentially nonoscillatory schemes for convection dominated problems, SIAM Rev. 51 (2009) 82–126.
[39] R. LeVeque, Finite Difference Methods for Ordinary and Partial Differential Equations, vol. 98, SIAM, Philadelphia, 2007.
[40] A.K. Henrick, T.D. Aslam, J.M. Powers, Mapped weighted essentially non-oscillatory schemes: Achieving optimal order near critical points, J. Comput. Phys. 207 (2005) 542–567.
[41] S. Tan, C.-W. Shu, Inverse Lax-Wendroff procedure for numerical boundary conditions of conservations laws, J. Comput. Phys. 229 (2010) 8144–8166.

[42] C.-W. Shu, High order WENO and DG methods for time-dependent convection-dominated PDEs: A brief survey of several recent developments, J. Comput. Phys. 316 (2016) 598–613.
[43] P.E. Souganidis, Approximation scheme for viscosity solutions of HJ equations, J. Differ. Equations 59 (1985) 1–43.
[44] S. Osher, C.-W. Shu, High-order essentially nonoscillatory schemes for HJ equations, SIAM J. Numer. Anal. 28 (1991) 907–922.
[45] A. Kurganov, S. Noelle, G. Petrova, Semidiscrete central-upwind schemes for hyperbolic conservation laws and HJ equations, SIAM J. Sci. Comput. 23 (2001) 707–740.
[46] J.D. Lawson, An order five Runge–Kutta process with extended region of stability, SIAM J. Numer. Anal. 3 (1966) 593–597.
[47] C.-W. Shu, S. Osher, Efficient implementation of essentially non-oscillatory shock-capturing schemes, J. Comput. Phys. 77 (1988) 439–471.
[48] S. Gottlieb, C.-W. Shu, E. Tadmor, Strong stability preserving high order time discretization methods, SIAM Rev. 43 (2001) 89–112.
[49] B. Gustafsson, H.O. Kreiss, J. Oliger, Time Dependent Problems and Difference Methods, John Wiley and Sons, 1995.
[50] R. Abgrall, Numerical discretization of the first-order HJ equation on triangular meshes, Comm. Pure Appl. Math. 49 (1996) 1339–1373.
[51] J.D. Lambert, Numerical Methods for Ordinary Differential Systems: The Initial Value Problem, John Wiley and Sons, New York, 1991.
[52] G. Diguet, E. Beaugnon, J.Y. Cavaillé, From dipolar interactions of a random distribution of ferromagnetic particles to magnetostriction, J. Magn. Magn. Mater. 321 (2009) 396–401.
[53] K. Danas, S.V. Kankanala, N. Triantafyllidis, Experiments and modeling of iron-particle-filled magnetorheological elastomers, J. Mech. Phys. Solids 60 (2012) 120–138.
[54] M.-A. Keip, M. Rambausek, A multiscale approach to the computational characterization of magnetorheological elastomers, Int. J. Numer. Meth. Eng. 107 (2016) 338–360.
[55] M.-A. Keip, M. Rambausek, Computational and analytical investigations of shape effects in the experimental characterization of magnetorheological elastomers, Int. J. Solids Struct. 121 (2017) 1–25.
[56] M. Labusch, J. Schröder, M.-A. Keip, An FE^2-scheme for magneto-electro-mechanically coupled boundary value problems, in: J. Schröder, D.C. Lupascu (Eds.), Ferroic Functional Materials: Experiments, Modeling and Simulation, Springer, 2018.
[57] W.F. Brown, Magnetoelastic Interactions, Springer-Verlag, Berlin, 1966.
[58] V. Lefèvre, O. Lopez-Pamies, Nonlinear electroelastic deformations of dielectric elastomer composites: II — Non-Gaussian elastic dielectric, J. Mech. Phys. Solids 99 (2017b) 438–470.
[59] B. Shrimali, V. Lefèvre, O. Lopez-Pamies, A simple explicit homogenization solution for the macroscopic elastic response of isotropic porous elastomers, J. Mech. Phys. Solids 122 (2019) 364–380.
[60] S.S. Demidov, The study of partial differential equations of the first order in the 18th and 19th centuries, Arch. Hist. Exact Sci. 26 (4) (1982) 325–350.